A Model for the Solubility of Minerals in Saline Aqueous Fluids in the Crust and Upper Mantle

by

Hanna Leigh Brooks

A thesis submitted in partial fulfillment of the requirements for the degree of

Master of Science

Department of Earth and Atmospheric Sciences
University of Alberta

ABSTRACT

Quantifying and predicting the dissolution of minerals in complex (multicomponent) aqueous fluids across wide ranges of *P-T* space is critical for interpreting geologic processes that involve water-rock interactions in the Earth's crust and upper mantle. Here, we define a new thermodynamic model for mineral solubility in saline aqueous fluids. The model is based on the coupling of two previous models: one for the solubility of minerals in pure H_2O fluids as function of temperature and pressure (Dolejš and Manning, 2010; *Geofluids*, **10**, 20-40), with the additional effects of fluid composition (salinity) modeled in part based on Akinfiev and Diamond (2009; *Geochimica et Cosmochimica Acta*, **73**, 1597-1608), with some additional modifications. Specifically, the new model adopts the approach of Akinfiev and Diamond (2009) to incorporate the effect of reduced H_2O activity in saline brines for reactions that involve hydration, and also adds new expressions for the equilibrium constants of reactions involving explicit sodium and/or chloride species. As such, the generic model is applicable to the solubility of minerals that dissolve as hydrous species, sodium and/or chloride species, and combinations thereof. The model has been calibrated against experimentally determined solubilities for five common rock-forming minerals – quartz, calcite, corundum, fluorapatite, and fluorite – in H_2O-NaCl solutions at temperatures up to 1100 °C and pressures up to 20 kbar. Data and trends observed in experimental measurements are well reproduced by our model predictions. In the case of pure H_2O fluids (zero salinity), the model is implicitly equivalent to the Dolejš and Manning (2010) model. The accuracy of the model is within both experimental uncertainties and accuracy ranges of the two models on which it is built. This thermodynamic model, accounting for dissolution reactions in multi-component fluids over an extreme range of *P-T-x* conditions, will allow for robust modeling of reactions and mass transport in natural systems.

PREFACE

This thesis is an original work by Hanna Brooks. No part of the thesis has been previously published.

For the ones who taught me to be curious,

To desire knowledge,

And ignited my love of the Earth

ACKNOWLEDGEMENTS

This research was supported in part by the US National Science Foundation under Grant No. EAR-1653977. Additional graduate support was provided by the Department of Earth and Atmospheric Sciences at the University of Alberta and the Department of Geosciences at the University of Arizona. I appreciate the continuous support and mentoring of Matthew Steele-MacInnis and Pilar Lecumberri-Sanchez through the turbulence of graduate school, and of my committee Bob Luth and Daniel Alessi. Thoughtful conversations with Frank Mazdab and careful reviews of experimental data sets and computer code by Jordan Jenson, Drew Barkoff, and Simone Runyon were critical to the success of the project. Special thanks to Benjamin Gruber for his careful and insightful reviews of the thesis.

TABLE OF CONTENTS

LIST OF TABLES

LIST OF FIGURES

1. INTRODUCTION

Modeling mineral solubility in fluids is a longstanding and critical issue in interpreting geological processes (e.g., Kennedy, 1950; Walther and Helgeson, 1977; Galvez et al., 2015). Chemical reactions and the transport of heat and materials in many geologic systems are driven and controlled by fluids. At deep crustal and upper mantle conditions, fluids – particularly concentrated salt solutions – play an important role in the initiation of many petrographic processes including regional metamorphism, metasomatism, and magma formation via partial melting (Aranovich and Newton, 1996). Elevated temperatures of these fluids, and lowered water activity because of salt dissolution, mobilizes alkalis, metals, REEs, and volatiles (Roedder, 1971; Aranovich and Newton, 1996). The ability of fluids to penetrate nominally impermeable rock through processes of induced porosity formation also implies that fluids exert a primary control in geodynamics (Putnis and Austrheim, 2010). Current approaches to thermodynamic modeling of mineral dissolution commonly invoke only simple, dilute H_2O or H_2O-CO_2 fluids. Fluid-inclusion studies, however, reveal that highly saline fluids are common in many environments including subduction zones (Manning, 2004; Spandler and Pirard, 2013), sedimentary basins (Cathles, 1990; Goldstein, 2001; Walter et al., 2017), magmatic-hydrothermal systems (White, 1974; Wilkinson, 2001; Groves et al., 2010; Rosenbaum et al., 1996; Frezzotti, 2001; Andersen and Neumann, 2001), deep crustal, orogenic and upper mantle settings (Touret, 2001; Newton and Manning, 2010; Putnis and Austrheim, 2010; Manning et al., 2013), and hydrothermal ore deposits (Wilkinson, 2001; Kesler, 2005; Bodnar et al., 2014). Thus, the effects of elevated salinity on mineral solubility are of key interest in many different settings.

High salinity brines can be generated by various mechanisms. In sedimentary basins, the original sedimentary environment of deposition may have been saline to hypersaline, owing for example to seawater evaporation (Hanor, 1994; Emsbo et al., 2016). Salinity may also be acquired post-deposition of sediments, for instance via retrograde hydration reactions in fluid-undersaturated environments (Yardley and Graham, 2002), or be a feature inherited from ancient connate fluids (e.g., Fritz and Frape, 1982). In other cases, salinity may be a primary feature of magmatic fluids, for instance, those fluids that are exsolved from granitic magmas (Frezzotti, 2001). Regardless of origin, dissolved salts in geologic fluids may have a variety of strong

effects on the properties of the fluid – ranging from effects on the density and phase equilibria (Bodnar, 2003), to effects on the activity and dielectric constant of water and, consequently, the hydration state and polymerization of dissolved species (Newton and Manning, 2010). Many metals and ions are complexed by Cl^- in saline aqueous fluids, and consequently, high salinity brines are commonly effective agents for mobilizing metals and dissolving various minerals (Yardley and Graham, 2002; Yardley, 2005; Newton and Manning, 2010). In addition, mixing high salt contents with gas-rich fluids commonly leads to immiscibility (e.g., Bowers and Helgeson, 1983) and partitioning of solutes between the immiscible fluids, which also affect mineral stability relations (Newton and Manning, 2010). Thermodynamic models that account for multi-component, multi-phase fluids are needed for robust modeling of reactions and mass/energy transport in natural systems.

The solubility of minerals in water and saline fluids has been the focus of numerous previous studies. Several of the key studies are summarized below, although this review is not exhaustive. In the case of mineral solubilities in pure H_2O, the recent study by Dolejš and Manning (2010) represents a key contribution. This is because their generic model (parameterized for seven minerals) is successful in modeling solubility from ambient conditions to pressures of 20 kbar and temperatures of 1100°C. In the case of saline solutions, Akinfiev and Diamond (2009) outlined an approach to modeling quartz solubility in complex multi-phase solutions (i.e. water ± salt ± gas), successfully capturing the effects of additional components over wide ranges of temperature (up to 1000°C), pressure (up to 10 kbar) and composition, although their model has not yet been extended to other minerals. As described in detail below, these two studies form part of the basis for our new model, which is capable of modeling the solubility of a variety of minerals in saline aqueous solutions. Below, we present a simple, generic approach to couple these previous models and extend them to dissolution reactions involving additional (sodium and/or chloride) species. This approach addresses the complexity of multiple mineral solubilities in H_2O-NaCl solutions across a wide range of geologically important P-T-x_{salt} conditions. By maintaining the simplicity of the model, and thereby minimizing the number of introduced fitting parameters, the resulting successful model yields results with more meaning to the geologic system and greater resiliency during interpolation and extrapolation (Akinfiev and Diamond, 2009).

2. FOUNDATIONS OF THE THERMODYNAMIC MODEL

This section briefly reviews and summarizes the aspects of previous solubility models pertinent to the development of our model. The first subsection deals with the solubility of minerals in pure H_2O, as this is a key starting point for modeling solubility of minerals in saline fluids. Quartz is used as a relatively simple example that has been the focus of many previous studies. The second subsection looks at solubility in H_2O-NaCl fluids, discussing the main complexities and the methods by which they are addressed, again focusing in part on quartz (especially, the model of Akinfiev and Diamond, 2009), but also on calcite as an additional example exhibiting contrasting behavior to that of quartz. In the subsequent section (Section 3), these previous approaches are tied together to create a new solubility model for minerals in saline fluids.

Two general modeling approaches have been employed in previous studies in order to describe thermodynamic interactions of aqueous species: 1) electrostatic and 2) density models. Although electrostatic models can be utilized to describe mineral-H_2O systems (i.e. Shock et al., 1989) and mineral-H_2O-non-polar gas systems (i.e. Xie and Walther, 1993; Akinfiev and Zotov, 1999) over a range of P-T-x_{gas} conditions, these models cannot be readily expanded to describe systems involving dissolved salts. As shown in preliminary modeling attempts by Akinfiev and Diamond (2009), simple electrostatic models have been found to be incapable of explaining the observed trends between quartz solubility and salt content at low pressures. Density models for mineral solubility in geologic fluids are based on empirical observations of correlations between fluid density, dielectric constant, and the solvation free energies of solutes. Previous studies have shown that density-based models can model mineral solubilities in mixed aqueous fluids accurately (see Akinfiev and Diamond, 2009), as well as in pure H_2O conditions. Therefore, a density-based approach is adopted for this study.

2.1 Solubility of Minerals in Pure H_2O

When considering the dissolution of a mineral in pure H_2O, a general reaction can be written representing the dissolution of i moles of a mineral to yield k moles of a single aqueous species,

$$i \text{ Mineral} + j\ H_2O = k \text{ (Aqueous Species)}, \qquad (1)$$

where the aqueous species produced may be a mixture of "free" species (ions, ion pairs, neutral complexes) and/or hydrous complexes (i.e. Kebarle, 1977; Pitzer, 1983; Borg and Dienes, 1992) with congruent mineral dissolution. In this generic reaction, dissolution of *i* moles of mineral yields *k* moles of aqueous species. In the absence of hydrous complexes, the stoichiometric coefficient *j* would be zero. Assuming that the mineral itself is a pure end-member (hence, assuming unit activity for the mineral), the equilibrium constant for this reaction is:

$$\mathrm{K} = \frac{a^{k}_{(\text{aqueous species})}}{a^{j}_{\mathrm{H2O}}}. \qquad (2)$$

Assuming that solubility is relatively low (as is the case for most silicates, oxides, carbonates), the activities of aqueous species can be approximated by their molalities and the activity of H_2O can be approximated as unity. In this case, Equation (2) can be written as:

$$m_{(\text{aqueous species})} = \mathrm{K}^{\frac{1}{k}}. \qquad (3)$$

From Equation (3), the molal concentration of the dissolved *mineral,* independently of the details of speciation, is directly proportional to the equilibrium constant, with the only complexity being the (unknown) ratio *1/k*. Crucially, thermodynamic formalisms allow us to define dissolution reactions such that $k = i$, yielding the convenient relationship that the equilibrium constant is equal to the molal concentration of the mineral. Ideally, there is a point where $k = i = 1$ for the reaction. If we defined the dissolution reaction differently (i.e., producing a different aqueous species), the only effect would be to adjust the value of the equilibrium constant by the exponent, *1/k*. In other words, thermodynamic formalisms obviate the need for detailed knowledge of the speciation, because the value of the equilibrium constant scales with the ratio 1*/k*. The molal concentration of the dissolved *mineral*, based on Equations (1) and (3) and the constraint $k = i = 1$, is related to the molal concentration of the produced aqueous speciecs but is additionally a function of the equilibrium constant:

$$m_{(\text{aqueous species})} = \text{K}. \qquad (4)$$

If we instead specified a different number of species produced in Equation (1), then we would adjust Equations (2)-(4) to account for the stoichiometry. But importantly, the equilibrium constant scales proportionately to the reaction stoichiometry, such that a thermodynamic model based on one reaction can be directly translated to accommodate a different stoichiometry by scaling K.

An additional consequence of Equation (3) is that solubility data for a mineral dissolved *in pure H_2O* provide no constraint on the stoichiometric coefficient *j* (moles H_2O participating in the dissolution reaction). Thus, with regards to the equilibrium constant expression, the coefficient *j* can be assumed zero (see Section 2.1.1). In this case, and adopting the constraint $k = i = 1$, the dissolution reaction can be rewritten as

$$\text{mineral}_{(\text{cr})} = \text{mineral}_{(\text{aq})}. \qquad (5)$$

where "mineral(cr)" is the crystalline form of the mineral and "mineral(aq)" is a hypothetical dissolved species with the exact stoichiometry of the mineral dissolving (e.g., Dolejš and Manning, 2010). This formalism is perfectly valid thermodynamically, for dissolution of a mineral in pure H_2O, and is consistent with the expression for the equilibrium constant, yielding the convenient expression (when i = k = 1):

$$\ln K = \ln m_{(\text{mineral})}. \qquad (6)$$

This approach may fail when solubility in saline solutions are considered, for two reasons (discussed in detail below, Section 2.2). Firstly, in saline solutions, the activity of H_2O (approximated by its mole fraction) is no longer unity, necessitating explicit treatment of the activity of water in Equation (2). In such cases, the coefficient *j* will be evaluated in light of solubility data in saline fluids. Secondly, for some minerals, additional aqueous species may be produced by interactions with dissolved salt/ions, implying additional reactants in Equation (1) or (as adopted here) additional speciation steps in the dissolution process. These topics are discussed in Section 2.2.

2.1.1 Solubility of Quartz in Pure H_2O

Many previous models have focused on quartz dissolution and the electrostatic interactions between aqueous silica and the surrounding water molecules. The Helgeson-Kirkham-Flowers (HKF) model (Helgeson et al., 1981) is perhaps the most successful model, widely used in geochemistry to predict the standard partial molal properties of aqueous ions and nonelectrolytes over a moderate range of *P-T* (up to 600°C and 5 kbar). In the model, solvation of the chemical potential of ionic species is defined by the Born equation (Born, 1920; Helgeson and Kirkham, 1976) and a quartz dissolution reaction involving no explicit H_2O, such that the dissolution has no bearing on the structure of aqueous silica nor on the structure of the solvent [Equation (7)].

$$SiO_{2\,(qtz)} = SiO_{2\,(aq)} \qquad (7)$$

Although many studies have discussed the explicit hydration of aqueous silica (commonly invoking the silicic acid species, $Si(OH)_4$), Equation (7) will implicitly yield identical results to a more explicit treatment of hydration, in the case of pure H_2O as described above. Manning (1994) devised a highly successful density-based model for quartz solubility, which operates based on the empirical observation that the standard state chemical potential of a solute is directly proportional to the logarithm of the density of pure H_2O (Marshall and Quist, 1967; Marshall and Franck, 1981). The model by Manning (1994), which is valid from the liquid-vapor curve of H_2O up to 1000°C and 10000 bar, has the form:

$$\log K = A\,(T) + B\,(T) \cdot \log \rho^{\circ}_{H_2O}, \qquad (8)$$

where ρ°_{H2O} is the density of pure H_2O and $A(T)$ and $B(T)$ are temperature-dependent polynomials:

$$A(T) = 4.260 - \frac{5764.2}{T} + \frac{1.7513\times10^{6}}{T^{2}} - \frac{3.3869\times10^{8}}{T^{3}} \qquad (9)$$

$$B(T) = 2.8454 - \frac{1006.9}{T} + \frac{3.5689 \times 10^5}{T^2} \qquad (10)$$

where T is in Kelvin. As described below (Section 2.2), the model of Manning [1994; Equations (8)-(10)] was adopted as part of the extension to H_2O-NaCl (and other) solutions by Akinfiev and Diamond (2009).

2.1.2 Generic Description of Solubility, Quartz plus Other Minerals, in Pure H_2O

Dolejš and Manning (2010) developed a new solubility model based on examination of the standard Gibbs energy of the dissolution reaction (Δ_{ds} G) and its relationship to the equilibrium constant K in pure H_2O. The model by Dolejš and Manning (2010) is similar to that by Manning (1994) for quartz (Section 2.1.1) but contains a different mathematical form for the temperature dependence and the temperature-density cross derivative, along with fewer empirical coefficients. The thermodynamic model of Dolejš and Manning (2010), parameterized for quartz, calcite, corundum, fluorapatite, fluorite, portlandite, and rutile, has the form:

$$\ln K = \left[\frac{-1}{R}\left(\frac{a}{T} + b + c \ln T + d\ T + e \ln \rho_{H_2O}\right)\right] \qquad (11)$$

where R is the gas constant ([8.314 J mol^{-1} K^{-1}]), T is absolute temperature (Kelvin), and ρ is pure H_2O density (g cm^{-3}) and a-e are mineral-specific coefficients fit to experimental data (Table 1). The model is valid up to 20 kbar and 1100°C (Dolejš and Manning (2010)).

2.2 Modeling Solubility in H_2O-NaCl Solutions

The approaches and models outlined in Section 2.1 for solubility of minerals in pure H_2O have many applications in geosciences, particularly in settings where aqueous fluids are dilute. But as noted above, saline fluids are common in many geologic settings and models for pure H_2O are inappropriate for modeling mineral solubility in such settings. In general, three main factors are expected to affect the predicted solubility of a mineral in saline fluids: Firstly, the addition of salt effectively reduces the activity of H_2O, which (in the case of reactions involving hydrous complexes) is a variable in the equilibrium constant [Equation (2)]. Secondly, as evident from Equations (8) and (11), when modeling solubility with density-based models, the density of

H_2O is an independent variable. Addition of NaCl is known to significantly modify the density of the resulting solution (e.g., Bodnar, 1983; Driesner, 2007). Thus, modification of solvent density with the addition of salt must also be considered in predicting solubility. Thirdly, in some cases, dissolved mineral species may interact with Na^+ and/or Cl^- to yield new, additional species, and these speciation reactions will enhance solubility. Each of these factors is discussed in the following three subsections. A modified version of Equation (1), including explicit treatment of NaCl in solution, is

$$i \text{ Mineral} + j \text{ } H_2O + q \text{ NaCl} = k \text{ (New Species)}. \qquad (12)$$

In this case, the species produced during dissolution may include "free" ions or neutral species, hydrous complexes, or complexes explicitly involving Na^+ and/or Cl^-. Different minerals may show fairly complex variation of salting-in and/or salting-out behaviors with the addition of NaCl, which depends on the nature of species formed and the variation in prevalence between species, as well as on the effects of salt on the activity of H_2O and the density of the solution (Xie and Walther, 1993; Newton and Manning, 2000; Newton and Manning, 2002; Tropper and Manning, 2007a; Antignano and Manning, 2008; Rapp et al., 2010). Salting-in is the effect where increasing the salt content, or ionic strength, of a solution results in an increase in solubility of a solute. Conversely, salting-out is the effect of decreasing the solubility of a solute with increasing salinity. For example, quartz solubility has been shown to exhibit salting-in behaviors, except in a restricted low *P-T* range around the critical point of water, where salting-out is present (Akinfiev and Diamond, 2009).

2.2.1 Effect of Dissolved NaCl on Activity of H_2O

In light of Equations (1) and (2), the effect of decreasing activity of water with the addition of NaCl must be incorporated into a solubility model for saline fluids. Evident from Equations (3)-(6), a hypothetical dissolution reaction assuming the stoichiometry of the dissolved species is equal to that of the mineral itself, which is perfectly appropriate for dissolution in pure H_2O, cannot capture this effect because the equilibrium constant of such a hypothetical reaction is independent of a_{H2O} [Equation (2)]. As such, in order to capture the effect of a_{H2O} on mineral solubility, the dissolution reaction must be rewritten to show dependence on solvation/hydration,

as in Equations (1) and (12). Unlike pure H_2O (See Section 2.1.2), the addition of solutes (e.g., NaCl) systematically lowers the value of a_{H2O} and affects the computed reaction quotient in Equation (2). For example, the reaction for quartz,

$$SiO_{2\,(qtz)} + n\ H_2O = SiO_2{\cdot}(H_2O)_{n\,(aq)} \qquad (13)$$

means the equilibrium constant for quartz solubility is:

$$K = \frac{a_{SiO_2{\cdot}(H_2O)_{n\,(aq)}}}{a^n_{H2O}}\ , \qquad (14)$$

The standard state definitions used here reference a_{H2O} to mole fraction (x_{H2O}) and activity of aqueous solutes to molal units. Therefore, assuming ideal behavior, $a_{H2O} = x_{H2O}$ and activity of the dissolved species is equal to their molality. Invoking the stoichiometric equivalence of one mole SiO_2 per mole $SiO_2{\cdot}(H_2O)_n$, allows us to express the molal concentration of SiO_2 as a function of the equilibrium constant K *and* mole fraction of H_2O:

$$\ln m_{SiO_2(aq)} = \ln K + n\ \ln x_{H_2O}. \qquad (15)$$

In the case where the coefficient $n = 0$ (no explicit hydration), then Equation (15) becomes identical to the simpler expression [Equation (6)] defined above for pure H_2O. Likewise, regardless of the value of n, when $x_{H2O} = 1$ (pure H_2O), the value of $\ln x_{H2O} = 0$ and Equation (15) again reverts to the simpler Equation (6). However, in the case of a NaCl (or other) solution, the value of x_{H2O} will always be <1, thus the value of ln (x_{H2O}) is negative and the molal solubility of quartz will be less than that in pure H_2O (assuming that the equilibrium constant is unchanged; see Section 2.2.2). This form of the dissolution reaction expression was adopted by Akinfiev and Diamond (2009). Analogous expressions can be written for other minerals.

2.2.2 Effect of Dissolved NaCl on the Solvent Density

When using a density model to describe mineral dissolution in multicomponent aqueous fluids, considerations must be taken to accommodate the effects of fluid components on the

physical properties of the solvent. For the system H_2O-NaCl, many empirical models are available to compute pressure-temperature-composition-density relationships over wide ranges of conditions (Section 4.7), so that the, density of the solvent can be calculated with reasonable accuracy. The more difficult question, however, is how to incorporate density of an H_2O-NaCl fluid into a density-based solubility model designed for pure H_2O. Fundamentally, density is simply the mass of fluid per unit volume, and there is no obvious *inherent* relationship between this parameter and the solubility of a mineral. Rather, the relationship arises from empirical observations of linear correlations between 1) the density and dielectric constant of H_2O (Yeats et al., 1971; Marshal 2008); and 2) the density of H_2O and the standard molal Gibbs free energy of solvation of a solute (Bischoff et al., 1986; Harvey and Levelt Sengers, 1990; Alvarez et al., 1994; Palmer et al., 2004). Consequently, the effect of solvent density in the case of saline solutions is not expected to follow the exact functional form as that for pure H_2O. Specifically, addition of NaCl to solution generally increases the solvent density at constant temperature and pressure, but may render the solvent a *less* effective dielectric medium, at odds with the density-permittivity relationships of pure H_2O (Helgeson et al., 1981; Driesner, 2007). Moreover, addition of NaCl to the solution may have a marked effect on the structure of H_2O (particularly at low pressure) and introduce competition for H_2O molecules that would otherwise be available for solvation of aqueous species produced by mineral dissolution. As such, it is reasonable to conclude that incorporating the effects of dissolved NaCl on the density-based correlations designed for pure H_2O would not be as simple as replacing the density of H_2O with the density of H_2O-NaCl in Equations (7) and (10). This conclusion is indeed confirmed by experimental observations and test calculations, which show that the density of a mixed H_2O-NaCl solvent is, in itself, a poor predictor for solubility of a mineral.

To capture the complexities of the relationships between NaCl concentration, solvent density, and solubility of quartz, Fournier (1983) introduced the concept of "density of free water." When a solution contains dissolved minerals, the water of hydration bound to dissolved species changes the weight fraction of "free" un-bound water in the solution available for interaction; thereby altering the density of the solution. This slight change in the definition of density accommodates changing fluid chemistry in the system and provides flexibility in the modeling of potential Na^+ and Cl^- complexing. Akinfiev and Diamond (2009) developed a density-based model for quartz solubility in fluids comprised of H_2O plus salts plus dissolved

gases [Equation (16)]. The model incorporates the solubility of quartz in pure H_2O based on the model of Manning (1994) [Equation (8)], with two important modifications. Firstly, the model deals with the effect of additional solutes on the activity of H_2O by addressing explicit solvation as described in the preceding section (Section 2.2.1). For this, the model assumes the aqueous silica species produced is $SiO_2 \bullet (H_2O)_2$ (or $Si(OH)_4$), thus $n = 2$ [Equations (13)-(15)] independent of temperature, pressure or composition (Table 2). Secondly, the model introduces a new parameter, V^*_{H2O}, to account for the effect of NaCl on the "density of free water". This V^*_{H2O} term is referred to as the "*effective molar volume of H_2O,*" and it is incorporated into the model of Akinfiev and Diamond (2009) as a fitting parameter:

$$\log m_{SiO_2} = A(T) + B(T) \cdot \log \frac{18.0152}{V^*_{H2O}} + 2 \log x_{H2O} \quad . \qquad (16)$$

Note that Equation (16) reverts to the model of Manning (1994) in the case of quartz dissolution in pure H_2O. The right-hand term in the equation, $+2\log(x_{H2O})$, accounts for explicit hydration as per Equations (13)-(15), and the term $18.0152/V^*_{H2O}$ is a modification of the solvent density [*c.f.* Equation (8)] invoking the effective molar volume of H_2O. Akinfiev and Diamond (2009) calculated the effective molar volume of H_2O from the molar volume of the fluid mixture (V_{mix}; $cm^3\ mol^{-1}$) according to the expression:

$$V_{mix} = x_{H2O} V^*_{H2O} + (1 - x_{H2O})\ V_s \qquad (17)$$

where V_s is defined and interpreted as an *intrinsic* volume of the solute (Akinfiev and Diamond, 2009). Akinfiev and Diamond (2009) estimated the value of V_s for NaCl by linear regression of quartz solubility data in saline fluids, but noted that the resulting value is closely approximated by the molar volume of molten salt ($V_{NaCl} = 30.8\ cm^3\ mol^{-1}$). Similarly, the value of V_s for molecular gases such as CO_2 is thought to be approximated by the excluded volume of the gas in a Redlich-Kwong-Soave type equation of state ($V_{CO2} = 29.9\ cm^3\ mol^{-1}$). According to Equation (17), V^*_{H2O} is related to, but distinct from, both the partial molar volume and apparent molar volume of H_2O in solution (see Akinfiev and Diamond, 2009 for details). This formulation by Akinfiev and Diamond (2009) is very successful in representing quartz solubility in saline and

gas-bearing fluids and, importantly, the predictability of V_s for a wide range of electrolyte and non-electrolyte solutes aids in robust extrapolation of this approach to multicomponent fluids.

In the formulation of the current model, the intrinsic volume term was reconsidered by plotting $x_{NaCl} \bullet V_{NaCl}$ versus mole fraction salt, x_{NaCl} (Figure 1). Experimental data from the SiO_2-H_2O-NaCl system reveals a curvature to the intrinsic volume trend at $n = 2$, as set by Akinfiev and Diamond (2009). To improve the fit, thereby straightening the line, n must be increased to ~4. Elimination of the intrinsic volume of NaCl from the model and manipulation of Equations (11) and (15) to solve for density allows for the prediction of ρ*, density of the fluid in the presence of brine. Prediction of the newly defined ρ* term was achieved by graphing ρF/ρ* versus x_{NaCl}, where ρF is density (ρ) multiplied by the mass fraction H_2O (F). At $n = 1.5$, experimental silica data from the H_2O-NaCl system yields a straight trend line with a slope of 1 (Figure 2). With the expression:

$$\frac{\rho \, \mathrm{F}}{x_{\mathrm{NaCl}}} = \frac{18.0152}{V_{\mathrm{Mix}}} \qquad (18)$$

we can simply use $18.0152/V_{Mix}$ as the predictor of density for the system H_2O-NaCl.

2.2.3 Speciation Reactions Involving Na^+ and/or Cl^-

In writing the dissolution reactions of minerals, in addition to hydration reactions (see above example of quartz, Section 2.2.1), some minerals may undergo additional speciation reactions involving Na^+ and/or Cl^-. In general, solutions may not have defined numbers of dominant solute species, nor are the identities of solute species necessarily identified. Nevertheless, additional speciation reactions involving Na^+ and/or Cl^- will generate enhanced solubility by driving the dissolution reaction towards the product side. Thus, if Na^+ and/or Cl^- species form, a one-step dissolution reaction as outlined in Equations (2), (3), and (6) will not capture the full solubility behavior. Detailed analysis of experimental solubility, however, can reveal trends indicative of particular solute species. For example, experimental data on corundum solubility generally shows solubility first increases with increasing salinity, then declining solubility with higher salinity (Newton and Manning, 2006). These trends suggest that the

produced Al-bearing solute species include Na^+ and/or Cl^- complexes (favored with increasing salinity) hydrous complexes (favored with decreasing salinity) (Newton and Manning, 2006).

As an example of mineral dissolution involving speciation reactions with Na^+ and Cl^-, consider the mineral calcite. Calcite dissolution yields predominately $CaCO_{3(aq)}$ ion pairs, which reacts with NaCl in solution to form calcium-chloride and sodium-carbonate species, as discussed in more detail below. Newton and Manning (2002) described this process by the reaction:

$$CaCO_{3\,(aq)} + 2NaCl_{\,(aq)} = CaCl_{2\,(aq)} + Na_2CO_{3\,(aq)} \qquad (19)$$

The equilibrium constant for this reaction is thus:

$$K_2 = \frac{m_{CaCl2}\, m_{Na2CO3}}{m_{CaCO3\,(aq)}\, m_{NaCl\,(aq)}{}^2} \qquad (20)$$

assuming $a_i = m_i$, and where the subscript "2" is included to indicate that this is a second step in the dissolution process. One implication of Equation (20) is that the concentration of calcium-chloride and sodium-carbonate species (thus, the net solubility of calcite) will be enhanced both by increased concentration of $CaCO_{3(aq)}$ (governed by the solubility product, or equilibrium constant "K_1" described below) *and* by increased salinity. Consequently, addition of NaCl is expected to yield enhanced solubility of calcite according to Equations (19) and (20) – calcite is expected to show salting-in, as is indeed observed in the experimental results (e.g., Newton and Manning, 2002) – although the effects of increased salinity on activity of H_2O and density of solvent must also be considered (Sections 2.2.1 and 2.2.2).

3. GENERAL MODEL FOR SOLUBILITY OF MINERALS IN H_2O-NaCl FLUIDS

In order to develop a new general model for the solubilities of minerals in saline geologic brines, we combined successful elements from thermodynamic modeling of minerals in pure H_2O from Dolejš and Manning (2010) [Equation (11)] with the density-based approach to quartz

solubility in multi-component fluids of Akinfiev and Diamond (2009) [Equation (16)]. In general, this coupling requires modification of the dissolution reactions assumed by Dolejš and Manning (2010) to account for explicit hydration, which exerts a strong control over the effect of NaCl on mineral solubility (Section 2.2.1). To this coupled expression, we append additional terms to account for solubility enhancement by formation of Na^+ and/or Cl^- complexes. Additional modifications include: 1) accounting for the density for H_2O-NaCl solutions [Section 2.2.2] and 2) activity of water [$n \ln x_{H2O}$, Equation (16)].

Flexibility is structured into the model as dissolution reactions for each mineral are not predefined nor are solute species assumed. The base expectation for dissolution is that the solid mineral will react with n moles of H_2O ($n \geq 0$) to produce new solute species [Equation (21)], and then these solute species react with q moles of NaCl to r moles of new solute species [Equation (22)].

$$\text{Mineral} + n\ H_2O = s\ \text{Species1} \tag{21}$$

$$\text{Species1} + q\ \text{NaCl} = r_1\ \text{Species2} + r_2\ \text{Species3} + \ \ldots r_z\ \text{SpeciesZ} \tag{22}$$

From experimental data and previous work, appropriate dissolution reactions for each mineral can be determined (Table 2). These generic equations can be combined to predict mineral solubility accurately in H_2O or H_2O-NaCl fluids. Chemical equilibria expressions can be written for the molality and mole fractions of products and reactants [Equations (23) and (25)], as well as the effects of density and temperature [Equations (24) and (26)].

$$K_1 = \frac{m^s_{\text{species1}}}{x^n_{\text{H2O}}} \tag{23}$$

$$\ln K_1 = \left[\frac{-1}{R}\left(\frac{a}{T} + b + c \ln T + d\ T + e \ln \frac{18.0152}{V_{Mix}}\right)\right] \tag{24}$$

$$K_2 = \frac{m^{r1}_{\text{species2}}\ m^{r2}_{\text{species3}} \ldots m^{rz}_{\text{speciesz}}}{m^s_{\text{species1}}\ m^q_{\text{NaCl}}} \tag{25}$$

$$\ln K_2 = \left[\left(\frac{a_2}{T} + b_2 + e_2 \ln\frac{18.0152}{V_{Mix}}\right)\right] \quad (26)$$

Fitted regressions of K_1 [Equation(11); Dolejš and Manning, 2010] and K_2 [Equation (26)] were used to calibrate the model for both pure H_2O and H_2O-NaCl systems and determine solubility products for five common rock-forming minerals – quartz, calcite, corundum, fluorapatite, and fluorite (Table 1).

A generic form of the model is written:

$$m_{Mineral\ [TOTAL]} = K_1\ x_{H2O}{}^{n} + K_1{}^{A}\ K_2{}^{A}\ m_{NaCl}{}^{B}\ x_{H2O}{}^{C} \quad (27)$$

$$A = \frac{1}{\sum_{i=1}^{z} r_i} \quad (28)$$

$$B = \frac{q}{\sum_{i=1}^{z} r_i} \quad (29)$$

$$C = \frac{n}{\sum_{i=1}^{z} r_i} \quad (30)$$

with values in *n* and *q* determined from experimental data and literature (Table 2). Quartz is an exception to Equations (28)-(30), because the values of A-C are all zero. Depending on the nature of the dissolution reaction, the specific mineral solubility equation may be simpler. For example, quartz dissolves in the presence of H_2O and is not affected by NaCl (Table 2), and the resulting dissolution equation is:

$$m_{SiO2\ [TOTAL]} = K_1\ x_{H2O}{}^{2} \quad (31)$$

Conversely, previous experiments (Fein and Walther, 1989; Aranovich and Newton, 1996) indicate calcite dissolves only in the presence of NaCl:

$$m_{\mathrm{CaCO3\ [TOTAL]}} = \mathrm{K}_1 + \mathrm{K}_1^{\frac{1}{2}}\,\mathrm{K}_2^{\frac{1}{2}}\,m_{\mathrm{NaCl}} \qquad (32)$$

The most complex case is for corundum which is reacts with H_2O and NaCl. In order to write a balanced equation, two H_2O reactions must occur for every one NaCl (See continued discussion in Section 5.3). The resultant dissolution reaction is:

$$m_{\mathrm{Al2O3\ [TOTAL]}} = \mathrm{K}_1^{\frac{1}{2}}\,x_{\mathrm{H2O}}^{\frac{3}{2}} + \mathrm{K}_1^{\frac{1}{2}}\,\mathrm{K}_2^{\frac{1}{2}}\,m_{\mathrm{NaCl}}^{\frac{1}{2}}\,x_{\mathrm{H2O}}^{\frac{3}{2}} \qquad (33)$$

Development and calibration of this model for specific minerals is fully outlined in Sections 4 and 5.

4. EXPERIMENTAL DATA SOURCES AND ANALYSIS

Solubilities of seven common rock-forming minerals – quartz, calcite, corundum, fluorapatite, fluorite, rutile, and portlandite – have been modeled across a wide range of geologically important *P-T* conditions in pure H_2O by Dolejš and Manning (2010). Therefore, in the present study we take the calibration of the model by Dolejš and Manning (2010) as a convenient starting point, and explore the extension of the solubility model to H_2O-NaCl fluids for these minerals. Portlandite had to be dropped from the present study, because we found no experimental data on portlandite in H_2O-NaCl fluids. Rutile also had to be excluded, because of the inconsistencies at pure H_2O conditions in the very small amount of available H_2O±NaCl data (Audétat and Keppler, 2005; Rapp et al., 2010). The other minerals – quartz, calcite, corundum, fluorapatite, and fluorite – are each described in more detail below. These minerals represent a rather diverse group in terms of dissolution behavior, with various minerals on this list dissolving primarily as either hydrous species or as associated ion pairs in pure H_2O, and some minerals on this list showing evidence of formation of sodium and/or chloride species, whereas others show no such propensity. Moreover, solubilities of minerals on this list vary by approximately eight orders of magnitude at a given pressure, temperature and composition condition. In compiling the data reported below, mineral solubilities reported from experimental studies were converted

to the molal concentration of the solute, salinity to mole fraction NaCl (with respect to H_2O+NaCl), experimental temperature to Kelvin, and experimental pressure to bar. Density of the solvent at experimental conditions was computed as described in Section 4.7. In cases where multiple experimental data points were available for the same experimental conditions (pressure, temperature, and fluid composition) for a given mineral, we averaged these data to a single value in order to avoid artificial weighting of the regression. During this averaging, if multiple experiments were done at equal pressure and temperature and similar (though not identical, within a tolerance of ± 0.1 wt.% NaCl) salinities, then fluid salinity was regarded as approximately equal and also averaged.

4.1 Quartz

The solubility of quartz in H_2O-silica fluids has been studied extensively from ambient conditions up to 1100°C and 20 kbar (e.g. Schloemer 1952; Hemley et al., 1980; Xie and Walther, 1993; Manning, 1994; Newton and Manning, 2000; Shmulovich et al., 2001; Shmulovich et al., 2006; Newton and Manning, 2008; Hunt and Manning, 2012). In the calibration for pure H_2O by Dolejš and Manning (2010), data from Hemley et al. (1980), Walther and Orville (1983), Manning (1994), and Fournier and Marshall (1983) were collected to produce a data set from 25 to 900°C and saturation vapor pressure to 20 kbar (n = 83). Other experimental data are reproduced remarkably well, even considering the small data set utilized in the fitted regression. For H_2O-NaCl-silica systems, published data from several experiments (Xie and Walther, 1993; Newton and Manning, 2000; Shmulovich et al., 2001; Shmulovich et al., 2006; Cruz and Manning, 2015) cover a wide range of *P-T-x* conditions. While fitting their H_2O-CO_2-NaCl-Silica model, Akinfiev and Diamond (2009), used data from Newton and Manning (2000) and Shmulovich et al. (2006). The dataset represents data from 400 to 900°C, from 1 to 15 kbar, and from 0 to 94 wt.% NaCl (n = 113). To model saline fluids for this study, data from Xie and Walther (1993), Newton and Manning (2000), Shmulovich et al. (2001), Shmulovich et al. (2006), and Cruz and Manning (2015) were used to build a data set covering 400 to 1100°C, 1 to 20 kbar, and 0.5 to 91 wt.% NaCl (n = 122; Appendix A).

4.2 Calcite

The solubility of calcite in pure H_2O was determined experimentally by Schloemer (1952), Morey (1962), Walther and Long (1986), Fein and Walther (1989), and Caciagli and Manning (2003). Dolejš and Manning (2010) regressed the results of Fein and Walther (1989) and Caciagli and Manning (2003) from 400 to 750°C and 2 to 16 kbar (n = 21). The exploratory studies of Schloemer (1952) and Morey (1962) were not used; nor were the data of Walther and Long (1986), who reported statistically lower solubilities than subsequent papers. In H_2O-NaCl aqueous solutions, experimental studies of Newton and Manning (2002) and Fein and Walther (1989) report mineral solubility. Dilute-H_2O experiments from Fein and Walther (1989) were not utilized in the calibration of the H_2O-NaCl model. The data of Newton and Manning (2002) were used to regress saline fluids from 700 to 900°C, from 6 to 14 kbar, and from 12 to 80 wt.% NaCl (n = 26; Appendix A).

4.3 Corundum

Dissolution of corundum in pure H_2O has been determined experimentally by the studies of Becker et al. (1983), Ragnarsdóttir and Walther (1985), Walther (1997), and Tropper and Manning (2007a). Dolejš and Manning (2010) calibrated their model fitting parameters for calcite using the results of Becker et al. (1983) and Tropper and Manning (2007a) at 660 to 1100°C and 2.5 to20 kbar (n = 24). They found that the two studies of Walther and others differ significantly from other published experimental data at similar *P-T* conditions, likely as a result of the formation of additional Al-bearing complexes during the course of experimentation (Dolejš and Manning, 2010). Because of these discrepancies, the two Walther papers were not used to check the reliability of corundum solubility in pure H_2O conditions. In H_2O-NaCl aqueous solutions, two datasets are available – Walther (2001) and Newton and Manning (2006). Data from Walther (2001) was found to show similar inconsistencies in predicted corundum solubility as the previous Walther experiments, therefore data from Newton and Manning was used at 800°C and 10 kbar, from 2 to 85 wt.% NaCl (n = 11; Appendix A).

4.4 Apatite

The solubility of apatite, namely Fluorapatite from Durango, Mexico, solubilities in both pure H_2O has been determined experimentally by Ayers and Watson (1991) and Antignano and Manning (2008). As noted by Antignano and Manning (2008), the experiment by Ayers and

Watson (1991) must be excluded on the grounds that the results are approximately one order of magnitude larger at 1 GPa, solubility trends are reversed from later work, and they report no change of solubility in the presence in brines. These discrepancies have been attributed by Antignano and Manning (2008) to errors in experimental design. Our model for pure H_2O conditions therefore used data at 700-900°C and 10-20 kbar (n = 6). Antignano and Manning (2008) and Mair et al. (2017) report solubilities of fluorapatite in brines. Data encompasses conditions of 10 to 77 wt.% NaCl, 7 to 15 kbar, and 700 to 900°C (n = 27; Appendix A).

4.5 Fluorite

The solubility of fluorite in pure H_2O and in brines has been determined in experiments by Strübel (1965) and Tropper and Manning (2007b). The earlier experiments of Strübel (1965) were conducted at low *P-T* conditions and have high analytical uncertainty. Tropper and Manning (2007b) measured solubility from 600 to 1000°C, 5 to 20 kbar with high precision and accuracy. Therefore, Tropper and Manning (2007b)'s data was used in the regressions for both pure H_2O by Dolejš and Manning (2010) (n = 12) and for H_2O-NaCl fluids in this study (n = 4). All data within the H_2O-NaCl system is at 800°C and 10 kbar and ranges from 26 to 75 wt.% NaCl salinity (Appendix A).

4.6 Fluid Properties

Many thermodynamic models are available for the volumetric properties of H_2O-NaCl fluids (e.g., Bowers and Helgeson, 1983; Anderko and Pitzer, 1993; Driesner, 2007), although none cover the full range of temperature (up to 1100°C), pressure (up to 20 kbar) and salinity (up to 97 wt.% NaCl) of the experimental data used here – especially with regard to the high pressures and salinities of some experiments (e.g., Cruz and Manning, 2015; Newton and Manning, 2006). Therefore, we designed an approach to compute density at such conditions assuming linear extrapolation of isochores from lower pressure and temperature. Our base model used density according to the models of Steele-MacInnis and Bodnar (2013) and Lecumberri-Sanchez et al. (2012), which compute fluid density along linear isochores (isochore dP/dT slopes according to Bodnar and Vityk, 1994 and Lecumberri-Sanchez et al., 2012) extending from the liquid-vapor envelope and halite liquidus surface, respectively. A Newton-Raphson iterative solver was used to locate the isochore that intersected the experimental pressure-temperature

point. The models used are relatively simple and empirical, yet comparison of these results with the density model of Driesner (2007) within its validity range showed an excellent ~1:1 match. The advantage of the method used here is that, because the isochores are inherently straight lines, they can be reliably extrapolated to high pressures (3 kbar; Lecumberri-Sanchez et al., 2012) to estimate density. Some of the experimental points could not be replicated by this method because fluid density was evidently outside the range of validity of these two models. These mostly comprised points at which salinity was low to moderate but fluid density was evidently either too 1) high, such that the relevant isochore originated on the ice or hydrohalite liquidus (not included in either of the aforementioned models); or 2) low, such that the relevant isochore originated near the critical point of the solvent, or on the dew-point curve side of the liquid-vapor envelope (again, not included in either model). In these cases, we used the model of Driesner (2007) if pressure was <5 kbar, and that of Sakuma and Ichiki (2016) if pressure was >5 kbar. For the few remaining points that were not captured by these methods, we used the model of Driesner (2007) to compute points along the relevant isochore between 2-5 kbar, and extrapolated the straight-line fitted to these points to the intersection with experimental pressure and temperature (by iterative solution). The temperature-pressure-salinity-density data used in this study are listed in Appendix A.

5. MINERAL-SPECIFIC SOLUBILITY MODELS

5.1 Quartz Dissolution Model

Critical analysis and modeling of the solubility of quartz in saline fluids by Akinfiev and Diamond (2009) indicates that the principal effects of increasing salinity are the reduction of H_2O activity and the modification of solvent density. They reported no evidence of formation of Na- or Cl-species, at least in terms of quality of fit to the experimental data. Equations (13) to (15) express the effect of x_{H2O} on quartz solubility as a function of explicit hydration of silica. The majority of experimental (Zotov and Keppler, 2002; Hashimoto, 1992) and modeling (Rustad and Hay, 1995; Sefcik and Goddard, 2001) studies indicate that over wide ranges of *P-T* conditions, the dominant silica species in solution is silicic acid $Si(OH)_4$ [i.e., $n = 2$ in Equation (16)]. There is some discussion in the literature of this specific hydration number however, with other studies indicating solvated silicic acid such as $Si(OH)_4 \bullet 2H_2O$ ($n = 4$; Shmulovich et al.,

2001). High-pressure, high-temperature experiments at conditions approaching the H_2O-saturated solidus of quartz also indicate that gradual polymerization of the silica species occurs with increased *P-T*. This transition implies that, as pressure and temperature increase, the incipient polymerization will yield silica dimers of the form $H_6Si_2O_7$ (or in structural formula, $(OH)_3SiOSi(OH)_3$) (n = 1.5) and at higher pressure and temperature the hydration number can be further reduced as polymerization proceeds. Consequently, it is plausible (indeed, likely) that the hydration number of aqueous silica in Equation (31) is a variable, ranging from values of4 or greater to 1.5 or less, depending on the *P-T* conditions.

The general dissolution equation [Equation (13)] does not consider the production of alkali and/or chloride species. Work on the dissolution of quartz in mixed fluid systems indicates that quartz may dissolve with water and salt in order to produce species such as alkali-silica hydrous complexes, which are *P-T* dependent first becoming detectable at ~300°C and becoming a strong presence in the fluid at high *P-T* conditions (Anderson and Burnham, 1983). Other studies have indicated that silicic acid and other more polymerized species may also undergo deprotonation to yield charged species at elevated pH (Hunt et al., 2011). These additional speciation steps were not found to be necessary to modeling quartz solubility in H_2O-NaCl fluids by Akinfiev and Diamond (2009), and the approach by Akinfiev and Diamond (2009) is adopted here. We revisited the possibility of alkali and/or chloride species in light of the comparison of predicted solubility with the experimental data, but found no indication of such species playing a significant role. As such, accounting for explicit hydration of aqueous silica appears to capture the major trends in quartz solubility in H_2O-NaCl fluids. This is an important factor in the development of our solubility model because it renders quartz solubility an ideal parameter in establishing the effect of fluid density on mineral solubility in saline fluids.

As discussed in Section 2.2.2, experimental data of mineral solubility for quartz in the H_2O-NaCl system was used to re-evaluate the density based on solving for the intrinsic volume of NaCl through plotting $x_{NaCl}V_{NaCl}$ vs x_{NaCl} at different values of n (Akinfiev and Diamond, 2009; Figure 1). Modification of the value of n set by Akinfiev and Diamond (n = 2) yielded an analysis of the "ρ*" using its relationship to ρF in ratio plotted versus x_{H2O} (Figure 2). Adjusting n to equal 1.5, density is predicted by the expression $18.0152/V_{Mix}$ for the system H_2O-NaCl. Modifying the density term modestly improved the RMSD value to 30.96, compared to 36.19 for the model of Akinfiev and Diamond (2009), and removed all adjustable parameters from the

density term. The value of $n = 1.5$ is consistent with a preponderance of dimers, $H_6Si_2O_7$, or only partially solvated silicic acid (mix of $SiO_{2(aq)}$ and $Si(OH)_4$) in the fluid. These hypotheses are broadly consistent with previous suggestions (see above). It is likely that this suggestion of a prevalence of dimers ($n = 1.5$) is strongly influenced by the high pressure, high-temperature quartz solubility data, and this result does not preclude the suggestion that pure silicic acid ($n = 2$) dominates at lower pressure and temperature. Nevertheless, a fixed value of $n = 1.5$ provides better overall predictive power than does $n = 2$ (note the improved RMSD compared to Akinfiev and Diamond, 2009) over the whole range of pressure and temperature considered here.

The final version of our model for the solubility of quartz in H_2O-NaCl fluids, coupling the models of Dolejš and Manning (2010) and Akinfiev and Diamond (2009), is expressed as Equation (31). Comparing the percent difference with experimentally determined solubilities for quartz, we see that our model predicts solubility with similar accuracy to the models of Akinfiev and Diamond (2009) and Dolejš and Manning (2010) (Figure 3A). Note, in the figures, percent error refers to:

$$\text{Error} = \left(\frac{\text{model solubility} - \text{experimental solubility}}{\text{experimental solubility}}\right) \times 100 \,. \qquad (34)$$

5.2 Calcite Dissolution Model

In the presence of pure H_2O, calcite can be modeled as a simple dissolution from a solid, directly to an aqueous phase, as there is no progressive hydration behavior as experienced by quartz:

$$CaCO_{3\,(s)} = CaCO_{3\,(aq)} \qquad (35)$$

$$\ln K_1 = \ln m_{CaCO3\,(aq)} \,. \qquad (36)$$

Therefore, Equation (36) is the same as used by Dolejš and Manning [2010; Equation (11)]. Newton and Manning (2002) found that, in the presence of a brine, calcite reacts with salt in order to produce Ca^{2+} and CO_3^{-} species [Equation (19)]. As salinity approaches concentrated conditions at high pressures and temperatures (up to 900°C and 15,000 bar), the dominant Ca^{2+}

solute product transitions to be $CaCl^+$ (Aranovich and Newton, 1996), whereas the carbonate species likely becomes $NaCO_3^-$ (Fein and Walther, 1989). We can simplify the K_2 expression [Equation (20)] with the assumption that:

$$m_{\mathrm{CaCO3\ [TOTAL]}} = m_{\mathrm{CaCO3\ [K1]}} + m_{\mathrm{CaCO3\ [EXTRA]}} \tag{37}$$

$$m_{\mathrm{CaCO3\ [EXTRA]}} = m_{\mathrm{CaCl2}} = m_{\mathrm{Na2CO3}}. \tag{38}$$

Now, a simplified expression for the dissolution of calcite can be written [Equation (32)], which allows us to thermodynamically model the dissolution of calcite for wide ranges of brine composition (Figure 3B). A multiple linear regression was calculated to predict K_2 based on 1/T and ln(ρ), using data from Newton and Manning (2002). A significant regression equation was found with an R^2 of 0.958.

5.3 Corundum Dissolution Model

In pure H_2O, corundum hydrates to form aluminum hydroxide:

$$\mathrm{Al_2O_{3\ (cor)} + 3\ H_2O = 2\ Al(OH)_{3\ (aq)}} \tag{39}$$

$$\mathrm{K_1} = \frac{m^2_{\mathrm{Al(OH)_3}}}{x^3_{\mathrm{H_2O}}}. \tag{40}$$

$$m_{Al_2O_3} = m_{Al(OH)_3}. \tag{41}$$

In pure H_2O, $x_{H2O} = 1$ and the K_1 is identical to the expression employed by Dolejš and Manning (2010). As salinity increases, x_{H2O} decreases and begins to affect K_1. An additional reaction occurs in brines,

$$\mathrm{2\ Al(OH)_{3\ (aq)} + NaCl_{\ (aq)} = NaAl(OH)_4 + Al(OH)_2Cl} \tag{42}$$

$$K_2 = \frac{m_{NaAl(OH)_4}\, m_{Al(OH)_2Cl}}{m^2_{Al(OH)_3}\, m_{NaCl}}, \quad (43)$$

with aluminum hydroxide and halite reacting to form Al ± Na ± Cl hydroxyl solute species (Newton and Manning, 2006). A full statement of corundum dissolution in the presence of both pure H_2O and brine solutions [Equation (33)], provides a basis for appropriate modeling of mineral solubility across a large volume of *P-T-x* space. Examining the error between predicted and experimental solubility at various experimental solubility points (Figure 3C), both the model of Dolejš and Manning (2010) and our model have similar residuals at pure H_2O conditions. A multiple linear regression of K_2 relied on the work of Newton and Manning (2006), based on 1/T and ln(ρ); with a significant regression equation having an R^2 of 0.977. The term 1/T was set to zero in the regression, as all of the experimental solubility data in brines has been conducted at 800°C.

5.4 Apatite Dissolution Model

In pure H_2O, solid apatite is hydrated to an aqueous species, and an expression for K_1 can be written:

$$Ca_5(PO_4)_6F_{2\,(Ap)} + H_2O = Ca_5(PO_4)_6F_2 \cdot H_2O_{\,(aq)} \quad (44)$$

$$K_1 = \frac{m_{Ca_5(PO_4)_6F_2\cdot H_2O\,(aq)}}{x_{H_2O}}. \quad (45)$$

As in the case of corundum, in pure H_2O, $x_{H2O} = 1$ and the K_1 is identical to the expression employed by Dolejš and Manning (2010). As salinity increases, x_{H2O} decreases and begins to affect the value of K_1. An additional reaction occurs with the addition of halite to the system:

$$Ca_{10}(PO_4)_6F_2 \cdot H_2O_{\,(aq)} + 3\ NaCl_{\,(aq)} = Ca_{10}(PO_4)_6F_2 \cdot H_2O \cdot 3NaCl_{(aq)} \quad (46)$$

$$K_2 = \frac{m_{Ca_{10}(PO_4)_6F_2\cdot H_2O\cdot 3NaCl_{(aq)}}}{m_{Ca_{10}(PO_4)_6F_2\cdot H_2O\,(aq)}\, m^3_{NaCl}}, \quad (47)$$

with the hydrated species reacting to form a new aqueous species (Mair et al., 2017). It is understood that the aqueous species produced in Equation (46) is not a valid aqueous species. It has been employed here, however, in order to maintain generality in the dissolution reaction and not predefine produced species (See above discussion in Section 2). A full statement for the dissolution of apatite in the presence of H_2O±NaCl fluids can be written:

$$m_{Ca_{10}(PO_4)_6F_2\ [TOTAL]} = K_1\ x_{H_2O} + K_1\ K_2\ x_{H_2O}\ m_{NaCl}{}^3. \quad (48)$$

In pure H_2O, the solubilities predicted by both our model and that of Dolejš and Manning (2010) have a similar accuracy (Figure 3D). A multiple linear regression was calculated to predict K_2 based on 1/T and ln(ρ), using data from Newton and Manning (2002). A significant regression equation was found with an R^2 of 0.721.

5.5 Fluorite Dissolution Model

In pure H_2O, fluorite dissolves to an aqueous phase, following the behavior of calcite, and an expression for K_1 can be written in the form of Equation (36). A second dissolution reaction step occurs in the presence of brines, where aqueous fluorite and halite react to produce Na^+ and Cl^- solute species (Tropper and Manning, 2007b):

$$CaF_{2\ (aq)} + NaCl_{\ (aq)} = CaClF^{\circ} + NaF^{\circ} \quad (49)$$

$$K_2 = \frac{m_{\ NaF^{\circ}}\ m_{\ CaClF^{\circ}}}{m_{CaF_{2\ (aq)}}\ m_{NaCl}}, \quad (50)$$

with a resultant equation for the dissolution of fluorite of:

$$m_{CaF_2\ [TOTAL]} = K_1 + K_1{}^{\frac{1}{2}}\ K_2{}^{\frac{1}{2}}\ m_{NaCl}{}^{\frac{1}{2}}. \quad (51)$$

In pure H_2O, the solubilities predicted by both our model and that of Dolejš and Manning (2010) have a similar accuracy (Figure 3E). At increased salinity, our model fits the small amount of

available experimental data with reasonable accuracy. A multiple linear regression was calculated to predict K_2 based on 1/T and ln(ρ) and a significant regression equation was found with an R^2 of 0.999. The term 1/T was set to zero in the regression, as all of the experimental solubility data in brines has been conducted at 800°C.

6. DISCUSSION

We modeled the experimental solubilities of quartz, calcite, corundum, fluorapatite, and fluorite in brine solutions with our new model to cover a temperature range of 100 - 1100°C and at pressures up to 20 kbar. Sources of localized larger error stem from scatter in solubility experimental data at a single *P-T* point and/or from error inherited from previous experimental procedures and individual experimental analytical techniques. Examining solubilities at set conditions offers a glimpse into the predictive and interpolation abilities of the new thermodynamic model, and points to the impact of aqueous speciation and ionic strength on observed trends.

In pure H_2O, the temperature-solubility (*T-x*) diagram for quartz shows a small temperature range which experiences retrograde silica solubility at 1 kbar (Figure 4). At 3 kbar (Figure 5), the diagram shows that the progressive addition of salt to the SiO_2-H_2O-NaCl system results in an increase in quartz solubility, especially at elevated temperatures, until 30 wt.% NaCl. Additional salt input (> 30 wt.% NaCl) decreases quartz solubility (salting-out) at the same *P-T* conditions. From the dissolution equation [Equation (13)], quartz reacts with water and no salt to produce new hydrous species. Solute silica is known to polymerize, especially at high *P-T* conditions, and may explain the prograde trends illustrating dramatic increases in solubility at high temperature and increased salinity (Zotov and Keppler, 2002; Newton and Manning, 2003, 2008b; Anderson and Burnham, 1983; Shmulovich et al., 2001). This behavior disappears by 3 kbar. At higher pressures (Figure 6, 5 kbar; Figure 7, 10 kbar), the quartz *T-x* diagrams all show prograde paths, with increasing solubility with increasing temperature. As salinity is increased however, the solubility of silica progressively decreases. This effect is more strongly observed at higher temperatures, where quartz is more soluble. The abrupt switch in the effect of NaCl addition on solubility illustrates a strong salting-out effect that controls quartz solubility above ~5 kbar.

The calcite *T-x* diagram at 1 kbar (Figure 8), has retrograde solubility conditions at low to moderate salinity (~10 wt.% NaCl) for temperatures between ~400 - ~600°C. Addition of NaCl decreases and then eliminates the retrograde solubility, while increasing the solubility of calcite in the $CaCO_3$-H_2O-NaCl system. At moderate to high salinities, high temperatures correspond with the highest modeled calcite solubilities. From Equation (19), calcite reacts with two moles of salt in brines to produce Ca and CO_3^- species. As pressure increases to 10 kbar (Figure 9 - 11, 3 - 10 kbar), solubility increases and the retrograde nature at lower salinities lessens. A noted shift in dominant solute species from low to high *P-T* (Newton and Manning, 2002; Aranovich and Newton, 1996; Fein and Walther, 1989) may be responsible for the change in prograde slopes at ~700 - 800°C observed at and above 3 kbar.

Dissolution of corundum in the system Al_2O_3-H_2O-NaCl [Equation (42)] results in similar behavior as calcite (i.e. Figure 8). With progressive increases in temperature and salinity, there are corresponding increases in solubility. Small scale retrograde behavior is observed as corundum dissolves in pure H_2O at 1 kbar (Figure 12). At pressures above 1 kbar, this retrograde trend is not seen (Figure 13 - 15, 3 - 10 kbar). Unlike the exponential curves seen for quartz, the slopes are more gradual at high temperatures. This phenomenon is likely due to the formation of new dominant solute species. A large increase in corundum solubility between pure H_2O and 10 wt.% NaCl can be seen at all four pressures studied. Care should be taken to not draw conclusions regarding this phenomenon, as the model has only been calibrated for salinity data at 800°C and 10 kbar, which excludes any T dependence from the model and forcing large extrapolation to pressures other than 10 kbar.

In the presence of H_2O±NaCl fluids, apatite dissolution results in retrograde solubility curves plotted on *T-x* diagrams at 1 - 10 kbar for salinities of 0 - 50 wt.% NaCl (Figure 16 - 19). Increases in salinity shifts the retrograde curve peak to higher temperatures. At all pressures, the model predicts increasing solubility with progressively increasing salinity. In some cases, this salting-in behavior is extreme from one salinity to another, as in the case from 40 wt.% to 50 wt.% NaCl at 1 kbar (Figure 16) and 3 kbar (Figure 17). Solubility increases by four orders of magnitude as pressure increases from 1 kbar (Figure 16) to 10 kbar (Figure 19).

Fluorite dissolution at 1 - 10 kbar (Figure 20 - 23) looks initially very similar to the retrograde curve plotted in *T-x* space for calcite, predictable as both minerals react with salt and no water to produce new solute species. Salting-in behavior is dominant with progressive salt

input producing higher fluorite solubilities, particularly at high temperatures. Only four experimental salinity data points exist for the system CaF_2-H_2O-NaCl at 800°C and 10 kbar; care should be taken to not draw many conclusions regarding model predicted solubility trends as more testing of the system needs to be completed to complete a full calibration.

Coupling multiple mineral solubility curves together allows us to examine how an aqueous fluid at specific *P-T-x* conditions impacts stable rock-forming minerals and provides an opportunity to model potential system behavior (Figure 24 A - C). Given the novel ability of our model to predict the solubility of common minerals in saline fluids across a wide range of geologically important *P-T* space, inherited errors accumulated by addition of numerous analytical models to examine solubility behavior across *P-T-x* ranges of model stability are eliminated. The solubilities of quartz, calcite, corundum, apatite and fluorite vary by eight orders of magnitude in molal concentration. Depending on salt concentration, the most soluble mineral fluctuates; whereas fluorapatite and corundum are consistently only slightly soluble, particularly at low temperatures. At high *P-T* conditions, calcite and fluorite exhibit salting-in behavior while quartz and corundum salt-out.

Overall, the trends observed in experimental measurements are well reproduced by our model predictions (Figure 24). The accuracy of the model is within both experimental uncertainties and accuracy ranges of the two models on which it is built. Further efforts to improve the accuracy may have to be primarily tied to future experimental work focused at covering gaps in *P-T-x* knowledge of mineral solubility.

7. GEOLOGIC APPLICATIONS

Application of this model of mineral solubility on natural systems provides an increased capacity for understanding the impacts of fluid migration within the crust and upper mantle. Saline fluids have been documented in many geologic environments and are often noted to play key roles in formation of system features and/or to drive formative processes. Increasingly, brines have been recognized by researchers as being important agents of rock alteration and mass transfer in high *P-T* metamorphic and magmatic systems. These fluids dissolve and transport large amounts of silicate constituents, other salt components, aluminum, and trace elements, such as rare-earth elements. Low to moderate salinity fluids have been recorded as the mineralizing

fluids in regional metamorphic metal deposits (McKeag and Craw, 1989; Robert et al., 1995; Dubé and Gosselin, 2007) and are essential for ore formation in hydrothermal porphyry deposits, where these fluids are capable of dissolving, transporting, and precipitating Au, Ag, Cu, W, Mb, and Pb (Hedenquist and Lowenstern, 1994; Weis, 2015). Saline fluids in sedimentary basins are also of societal interest. Common occurrence of brines with gas exploration and recent increase of oil production in salt traps has called into focus the importance of salt on these resources. Additionally, calcite and fluorite veins in Mississippi Valley Type deposits, shale-hosted Pb, Zn, and Ba deposits, copper rift basin redbed deposits, and sandstone-hosted uranium deposits all invoke brines as ore-forming fluids (Hanor, 1994). Evidence for fluid flow at high *P-T* conditions is seen as corundum veins in deep crustal rocks (e.g. Mercier et al., 1999).

Brines also play an important role in heat and material transfer in subduction zone environments, having the ability to transport high-field strength, large-ion lithophile, and light-rare-earth elements as dissolved species during the progressive dehydration of the slab (Philippot and Selverstone, 1991; Gao et al., 2007). These trace elements are seen precipitated bound in the structure of rutile crystals (Gao et al., 2007). Interaction of these *HP-LT* subduction zone rocks with fluids of various compositions could play a dramatic effect on stable mineral phases, resultant metasomatic effects of dissolved species, and differing heat capacities of fluids based on composition (Philippot and Selverstone, 1991).

8. CONCLUSIONS

1) We have developed a new thermodynamic model for the solubility of minerals in saline fluids up to 20 kbar and 1100°C. This simple, generic model succeeds in modeling the intricacy of common minerals dissolving in a complex aqueous fluid in geologically important *P-T* ranges. Results of the modeling can be used for robust modeling of reactions and mass/energy transport in natural systems and to glean a greater understanding of the importance of fluid movements in geologic systems.

2) The model was calibrated with the solubilities of five common rock-forming minerals – quartz, calcite, corundum, apatite, and fluorite. Modeled solubilities were compared to the extant database of experimental data, spanning from 100 – 1100°C and ~1 – 20 kbar. Coupling multiple

mineral solubility curves together allowed examination of the potential impact of an aqueous fluid at specific *P-T-x* conditions on the solubility of common minerals. Depending on salt concentration, the identity of the most soluble mineral fluctuates; salting-in and salt-out behaviors were both noted depending on mineral type and *P-T* conditions.

3) Examining solubility (*T-x*) diagrams for each mineral show that, in general, increasing salinity, temperature, and/or pressure in the system leads to a corresponding increase in solubility. However, in-depth examination of these diagrams illustrates that the effect is dependent on temperature, pressure, the formation of solutes, and the electrostatic behavior of the solution (i.e. salting-in and salting-out). Which of these variables dominates varies as a function of mineral properties and *P-T-x* conditions.

4) Application of this new mineral solubility model to natural systems provides an increased capacity for understanding the impacts of fluid migration within the crust and upper mantle. This model encompasses H_2O±NaCl fluids in a wide range of scientifically and societally important geologic settings (e.g. hydrothermal porphyries, sedimentary basins, and subduction zones).

5) Due to the "simple" nature of the model, extrapolation and interpolation of data is possible with a high degree of accuracy over an extremely wide range of crustal to upper-mantle pressures and temperatures, and a large range of brine concentrations. Modeling of numerous, diverse geologic settings (i.e. sedimentary basins, subduction zones, hydrothermal ore deposits) is possible via a single, coherent analytical model.

6) Future studies building upon this generic model of mineral solubility in H_2O±NaCl fluids might first focus on the incorporation of additional salt species in the fluid. Additional fluid complexity of interest will be the incorporation of gases (i.e. CO_2, CH_4, and N_2) in to the model, as many natural geologic fluids lie along the H_2O+gas binary. Of particular interest will be the expansion of the model to incorporate the impact of a fluid on the dissolution of a system of minerals (i.e. the system H_2O-NaCl-SiO_2-Al_2O_3), and the potential bearing on solubility trends compared to the independent fluid-mineral modeling performed in this study.

Table 1: Model Fitting Parameters for K1 and K2.

	a (J/mol)	b (J/K mol)	c (J/K mol)	d (J/K mol)	e (J/K mol)	Data Source	a_2 (J/mol)	b_2 (J/K mol)	e_2 (J/K mol)	Data Source
Apatite-F	63400	3.9			-89.32	1	-9332.343	8.190	9.381	1, 2
Calcite	57400	-35.71			-72.98	3, 4	-8340.197	3.762	-9.462	5
Corundum	80300	-29.31			-37.01	6, 7	0	-5.372	0.550	8, 9
Fluorite	56400	-24.89			-59.73	10	0	-3.799	-15.142	10
Quartz	23600	-52.92	10.93	-0.0463	-18.52	11-14	-	-	-	15-19

Sources of Experimental Data: 1- Antignano & Manning (2008); 2- Mair et al (2017); 3- Fein & Walter (1989); 4- Caciagli & Manning (2003); 5- Newton & Manning (2002); 6- Becker et al. (1983); 7- Tropper & Manning (2007a); 8- Walther (2001); 9- Newton & Manning (2006); 10- Tropper & Manning (2007b); 11- Hemley et al. (1980); 12- Fournier & Marshall (1983); 13- Walther & Orville (1983); 14- Manning (1994); 15- Xie and Walther, 1993; 16- Newton and Manning, 2000; 17- Shmulovich et al., 2001; 18- Shmulovich et al., 2006; 19- Cruz and Manning, 2015

Table 2: Dissolution Equations Utilized for Mineral Solubility Modeling.

	Mineral Dissolution Formula Taken from Literature	Data Source
Apatite-F	$Ca_{10}(PO_4)_6F_2$+ 3NaCl + H_2O = k solute species	1
Calcite	$CaCO_3$+ 2NaCl = $CaCl_2$ + Na_2CO_3	2, 3
Corundum	Al_2O_3 + 3H_2O = $Al(OH)_3$ 2$Al(OH)_3$ + NaCl = $NaAl(OH)_4$ + $Al(OH)_2Cl$	4
Fluorite	CaF_2+ NaCl = CaClF° + NaF°	5
Quartz	SiO_2+ nH_2O = $SiO_2 \cdot (H_2O)_{n\ (aq)}$	6

Data sources: 1- Mair et al. (2017); 2- Aranovich & Newton (1996); 3- Fein & Walther (1989); 4- Newton & Manning (2006); 5- Tropper & Manning (2007b); 6- Akinfiev & Diamond (2009)

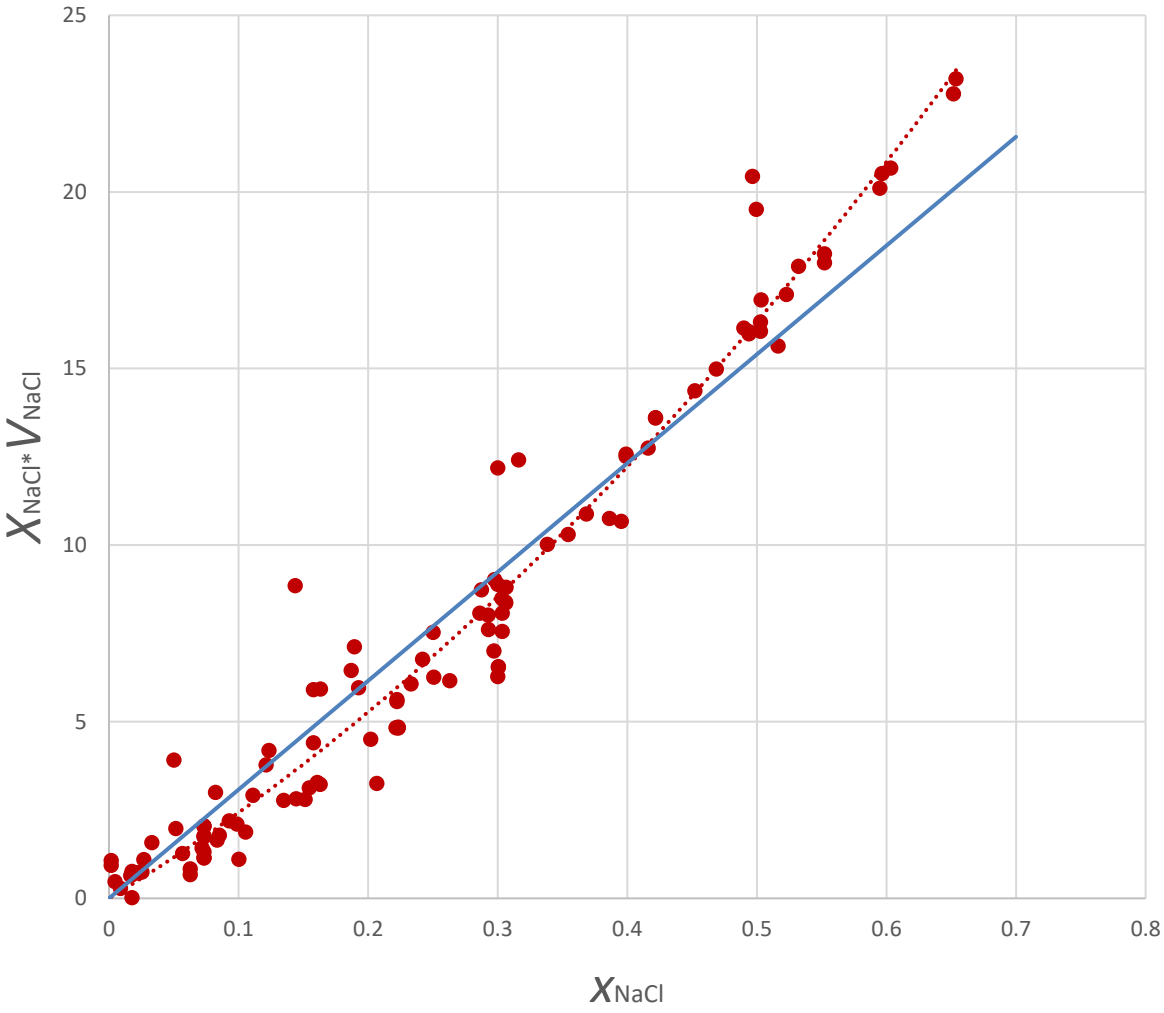

Figure 1: Re-calculation of the intrinsic volume, V_{NaCl}, defined by Akinfiev and Diamond (2009), by plotting $x_{NaCl} \bullet V_{NaCl}$ versus x_{NaCl}. In order to fit a straight line and calculate V_{NaCl}, the value of n must be set to ~4. This change forces V_{NaCl} from 30.8 $cm^3\ mol^{-1}$, reported by Akinfiev and Diamond (2009; blue line), to 27.5 $cm^3\ mol^{-1}$. Due to these inconsistencies in V_{NaCl}, alternative methods to account for density modification with addition of NaCl to H_2O fluids were explored.

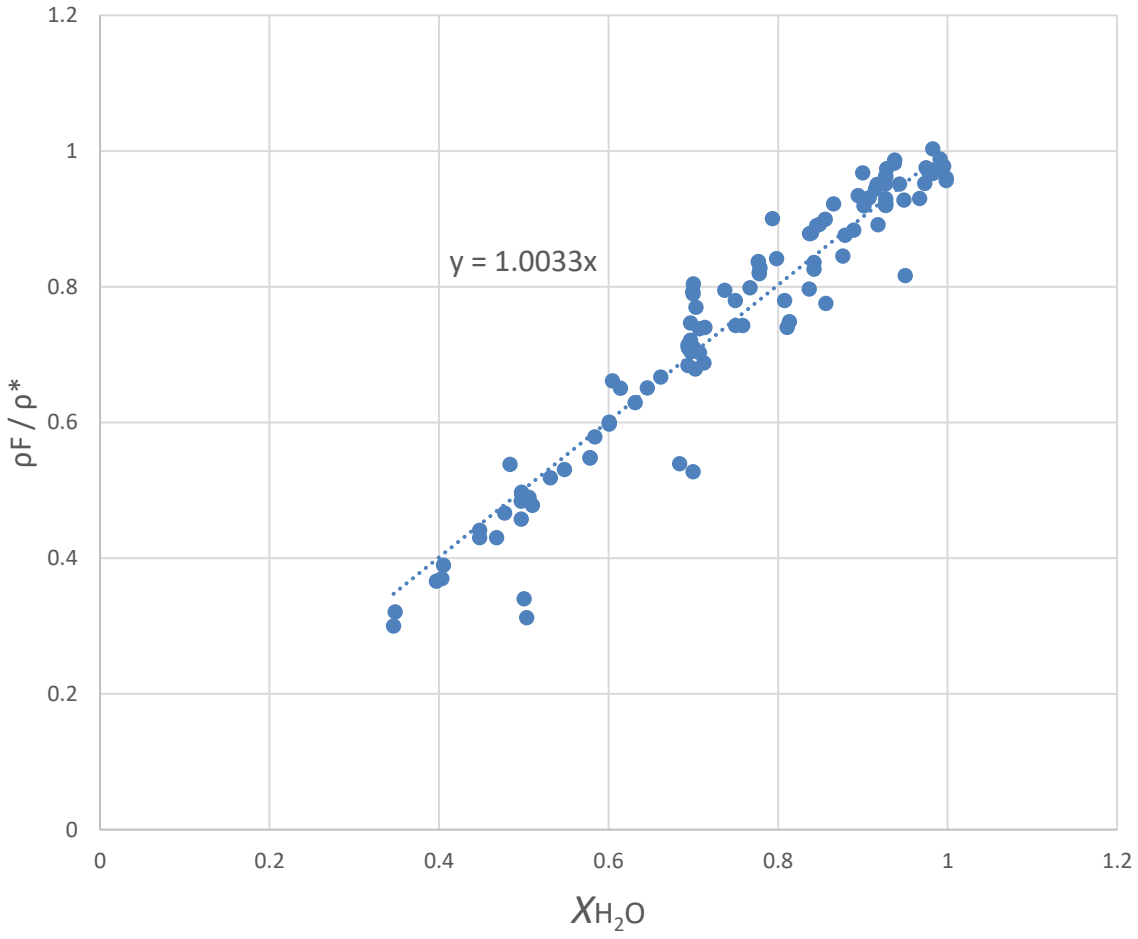

Figure 2: Graph of ρF/ρ* versus x_{H2O}, where ρF is density (ρ) multiplied by the mass fraction H_2O (F). When n = 1.5, the theoretical hydration number of the dimer, the plot yields a straight line with a slope = 1. With n = 1.5 and an expression relating density, composition, and volume, elimination of V_{NaCl} from the model can occur by simply using $18.0152/V_{Mix}$ as the predictor for density.

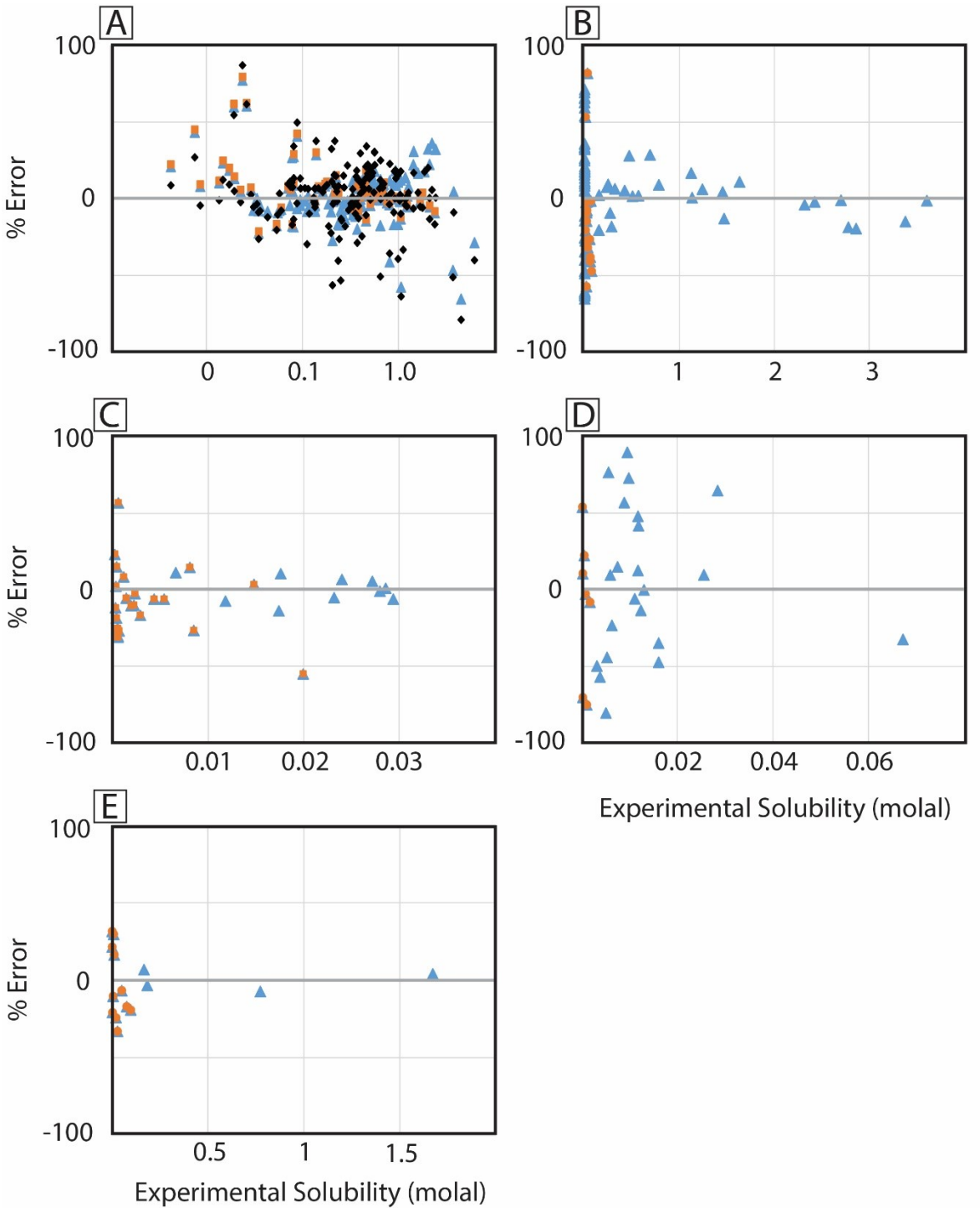

Figure 3 A-E: Percent error between model predicted solubility and experimental solubility plotted against experimental solubility for A) Quartz, B) Calcite, C) Corundum, D) Fluorapatite, and E) Fluorite; this study (in blue) shown compared with Akinfiev and Diamond (2009; in grey) and Dolejš and Manning (2010; in orange).

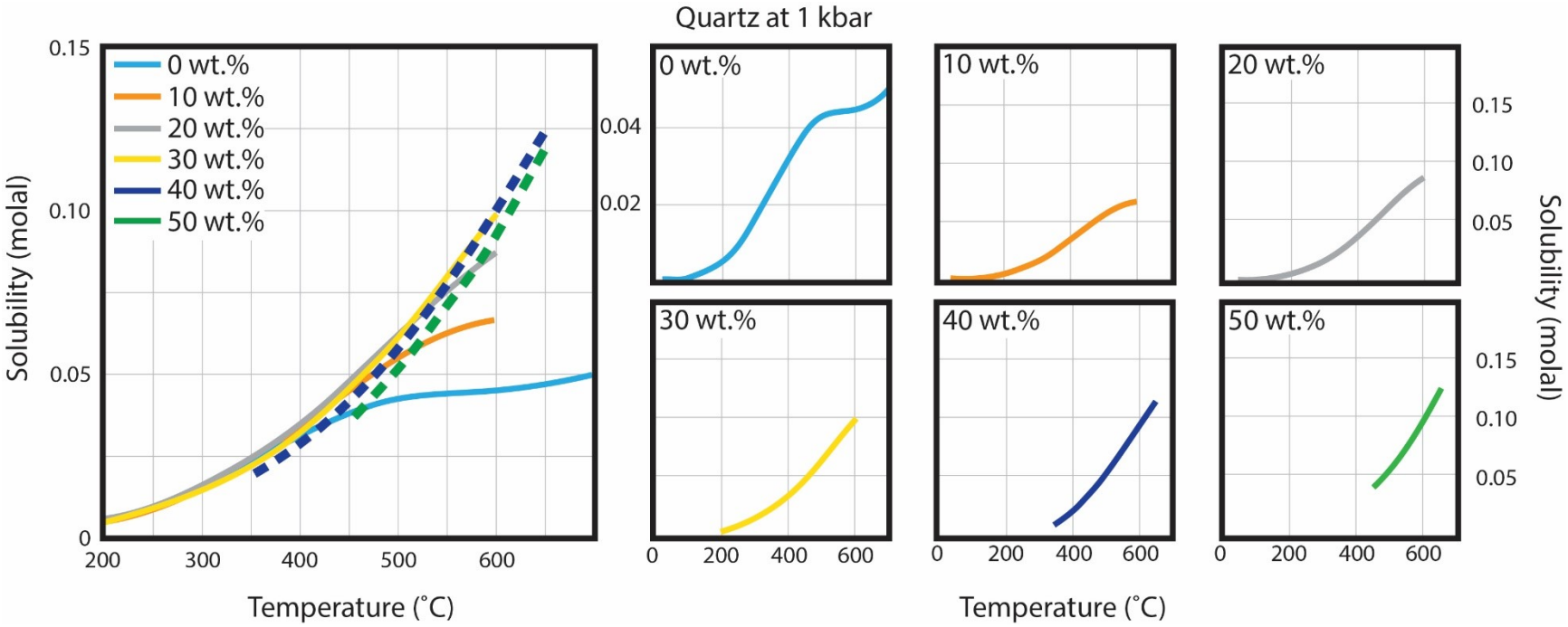

Figure 4: *T-x* diagram illustrating the effect of temperature and salinity on quartz solubility in H_2O±NaCl fluids at 1 kbar. Retrograde solubility is evident at pure H_2O conditions, transitioning to prograde solubility trends with increasing salinity. Solubility increases progressively until 40 wt.% NaCl, afterwards salting out is observed.

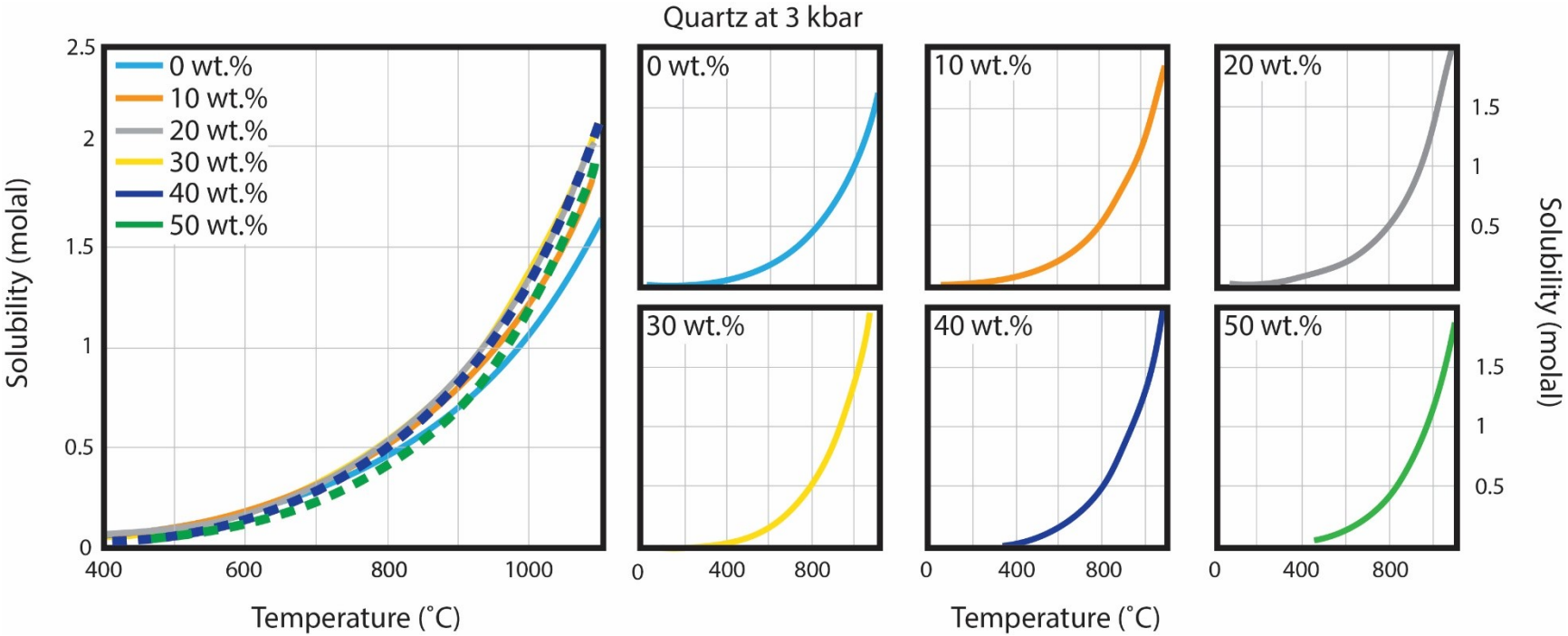

Figure 5: *T-x* diagram illustrating the effect of temperature and salinity on quartz solubility in H_2O±NaCl fluids at 3 kbar. Solubility increases progressively until 40 wt.% NaCl, afterwards salting out is observed. Solubility increases progressively with increasing temperature, producing prograde solubility trends.

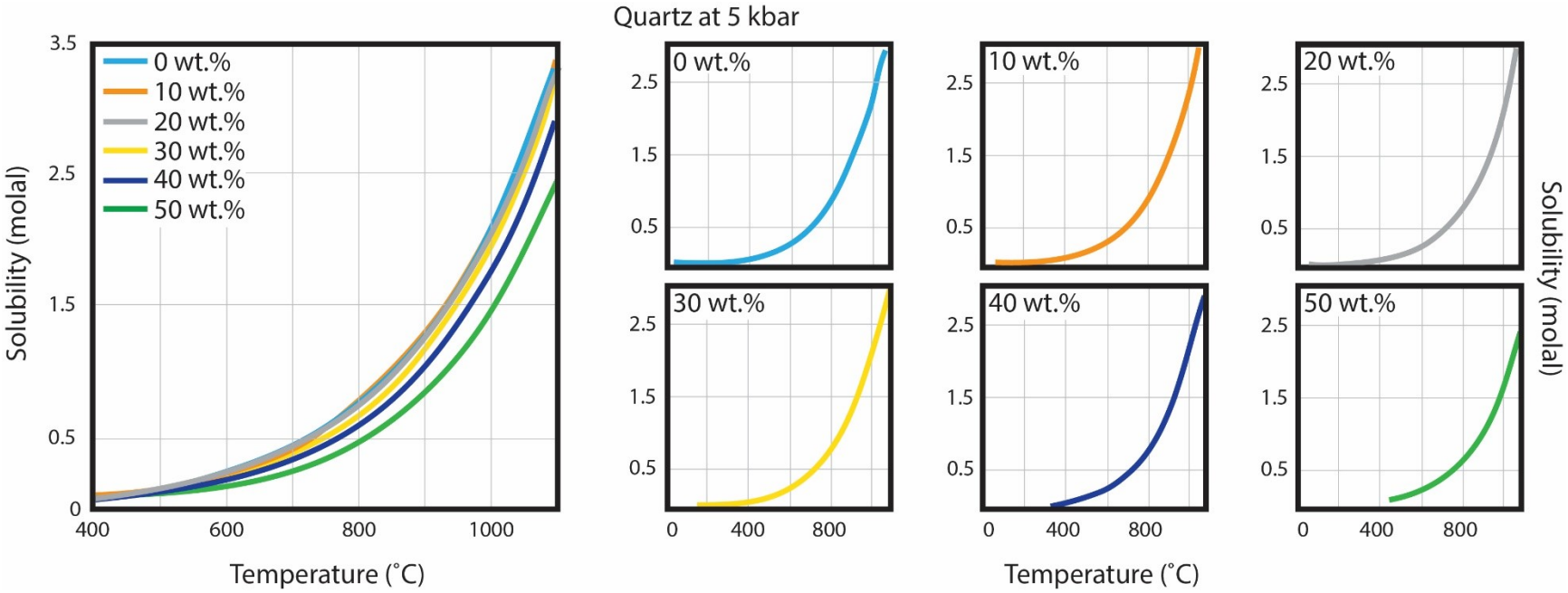

Figure 6: *T-x* diagram illustrating the effect of temperature and salinity on quartz solubility in H_2O±NaCl fluids at 5 kbar. Salting out behavior and prograde solubility trends are observed across all modeled *P-T-x* conditions.

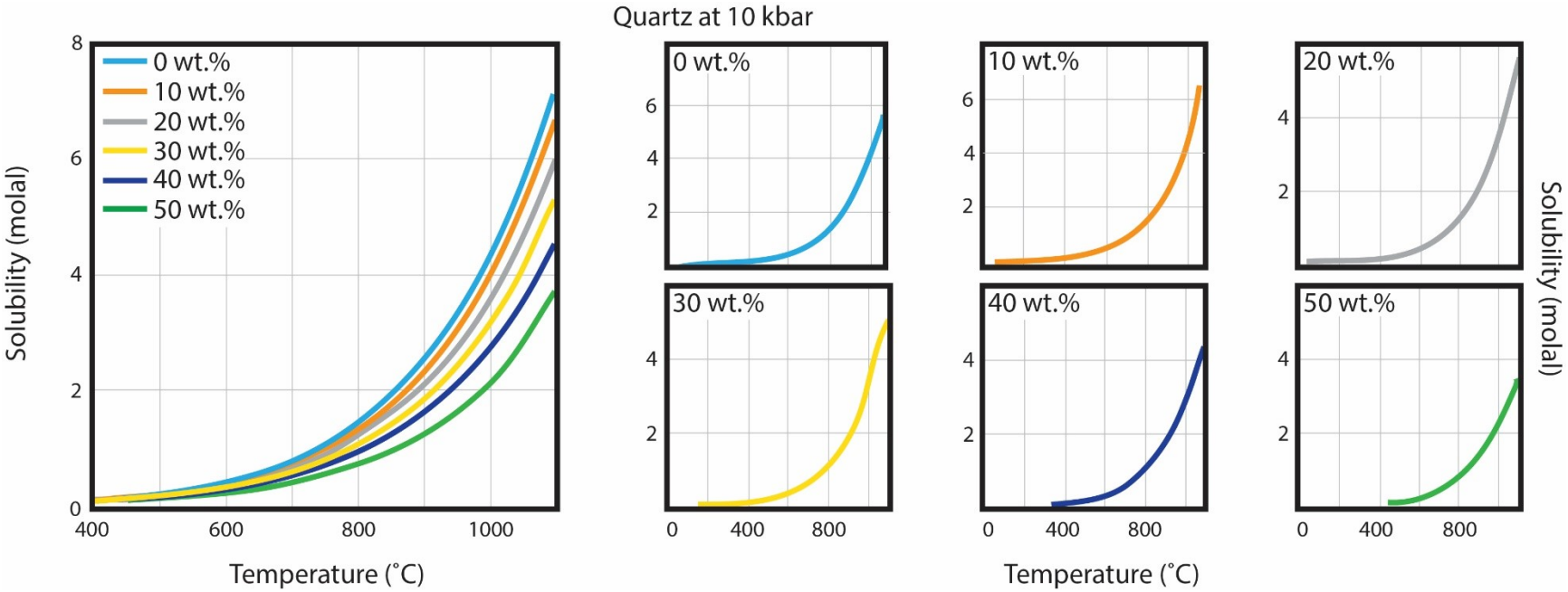

Figure 7: *T-x* diagram illustrating the effect of temperature and salinity on quartz solubility in H_2O±NaCl fluids at 10 kbar. Salting out behavior is observed across all modeled *P-T-x* conditions, with increasing salinity driving a decrease in solubility regardless of temperature. Prograde solubility trends are modeled for all salinity conditions.

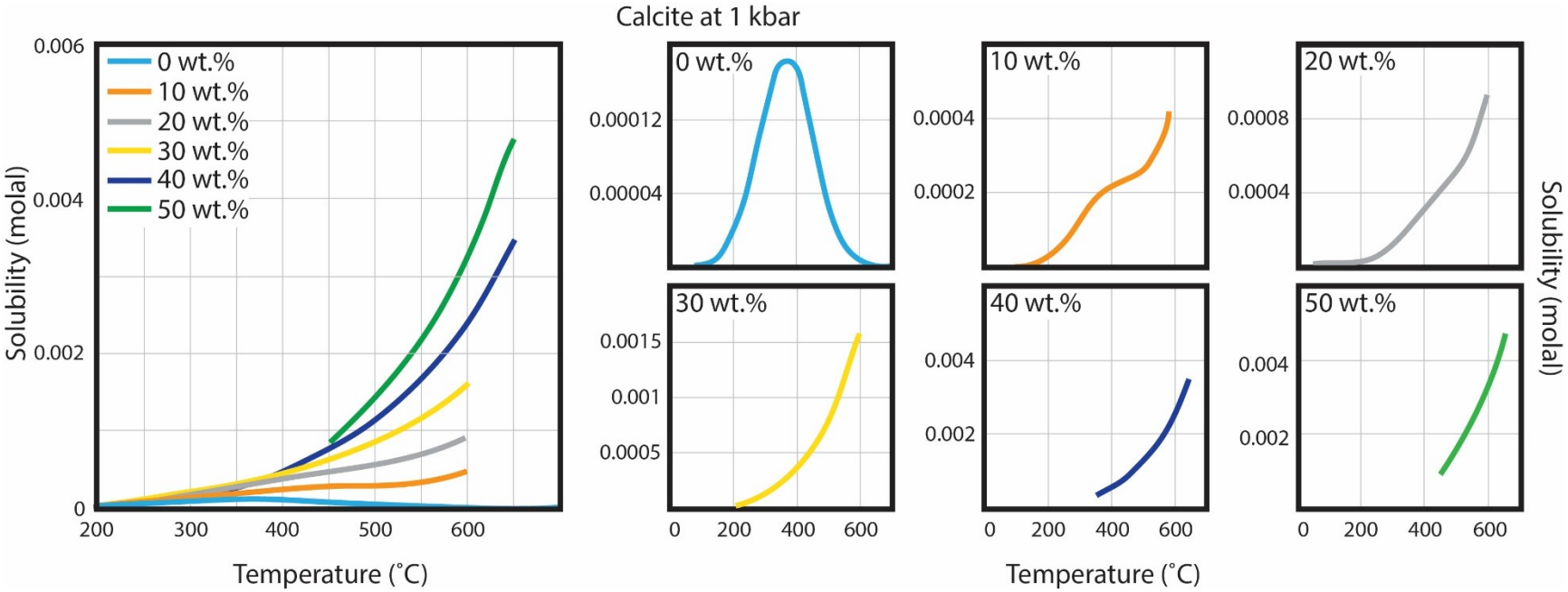

Figure 8: *T-x* diagram illustrating the effect of temperature and salinity on calcite solubility in H_2O±NaCl fluids at 1 kbar. Solubility increases progressively with increasing salinity. Retrograde solubility trends are seen in pure H_2O conditions, grading to fully prograde by ~30 wt.% NaCl salinity.

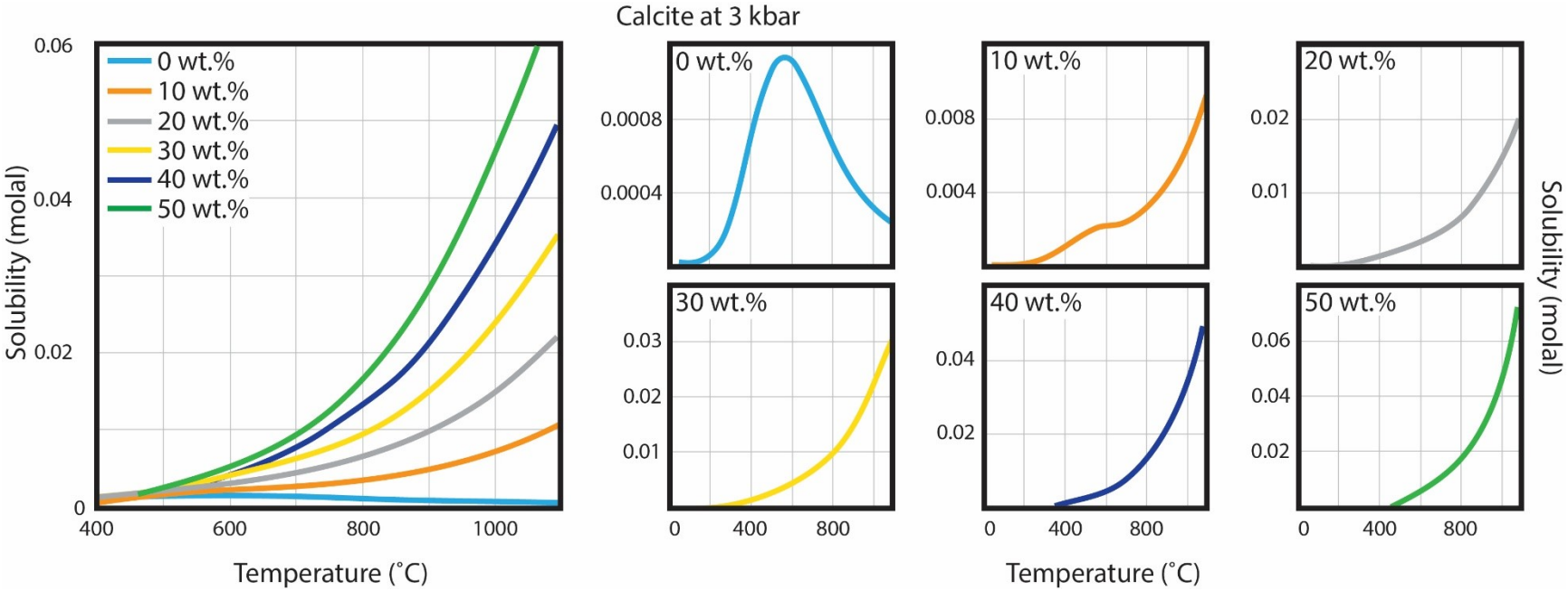

Figure 9: *T-x* diagram illustrating the effect of temperature and salinity on calcite solubility in H_2O±NaCl fluids at 3 kbar. Solubility increases progressively with increasing salinity. Retrograde solubility trends are seen in pure H_2O conditions, grading to fully prograde by ~20 wt.% NaCl salinity, and are more gradual than those seen at 1 kbar conditions.

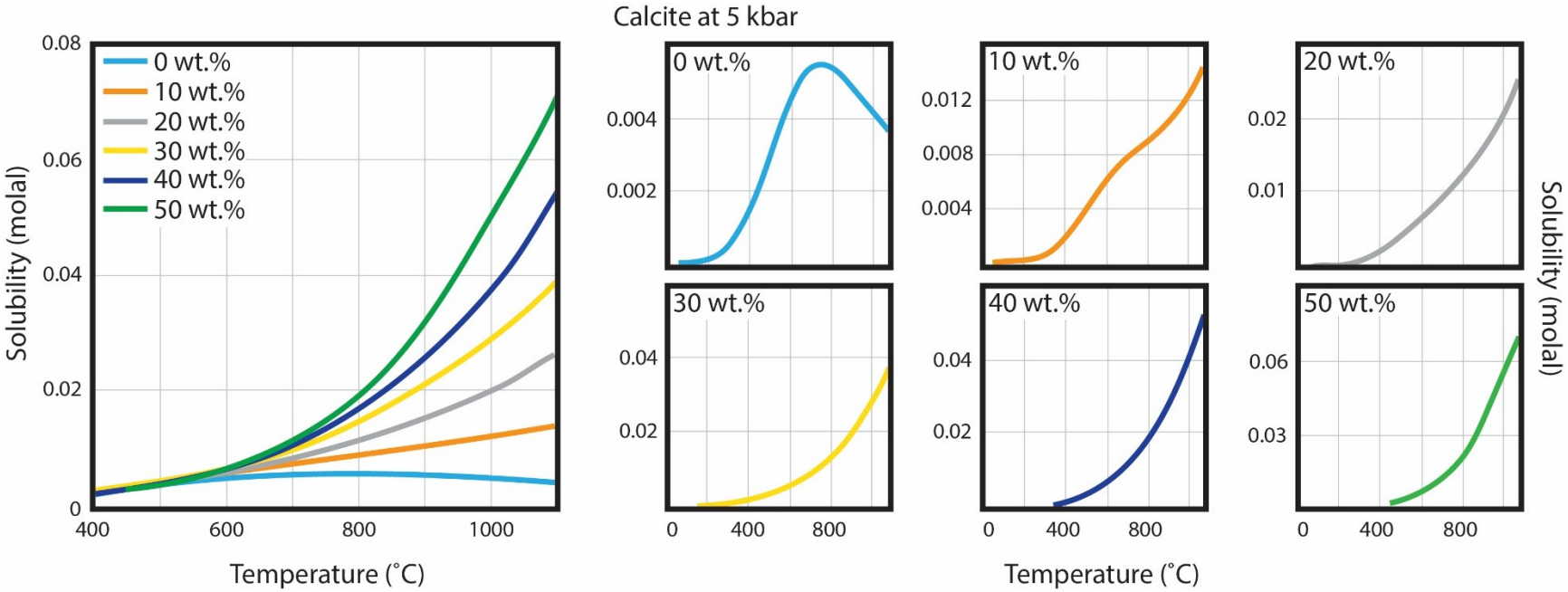

Figure 10: *T-x* diagram illustrating the effect of temperature and salinity on calcite solubility in H_2O±NaCl fluids at 5 kbar. Solubility increases progressively with increasing salinity. Retrograde solubility trends are seen in pure H_2O conditions, grading to fully prograde by ~10 wt.% NaCl salinity.

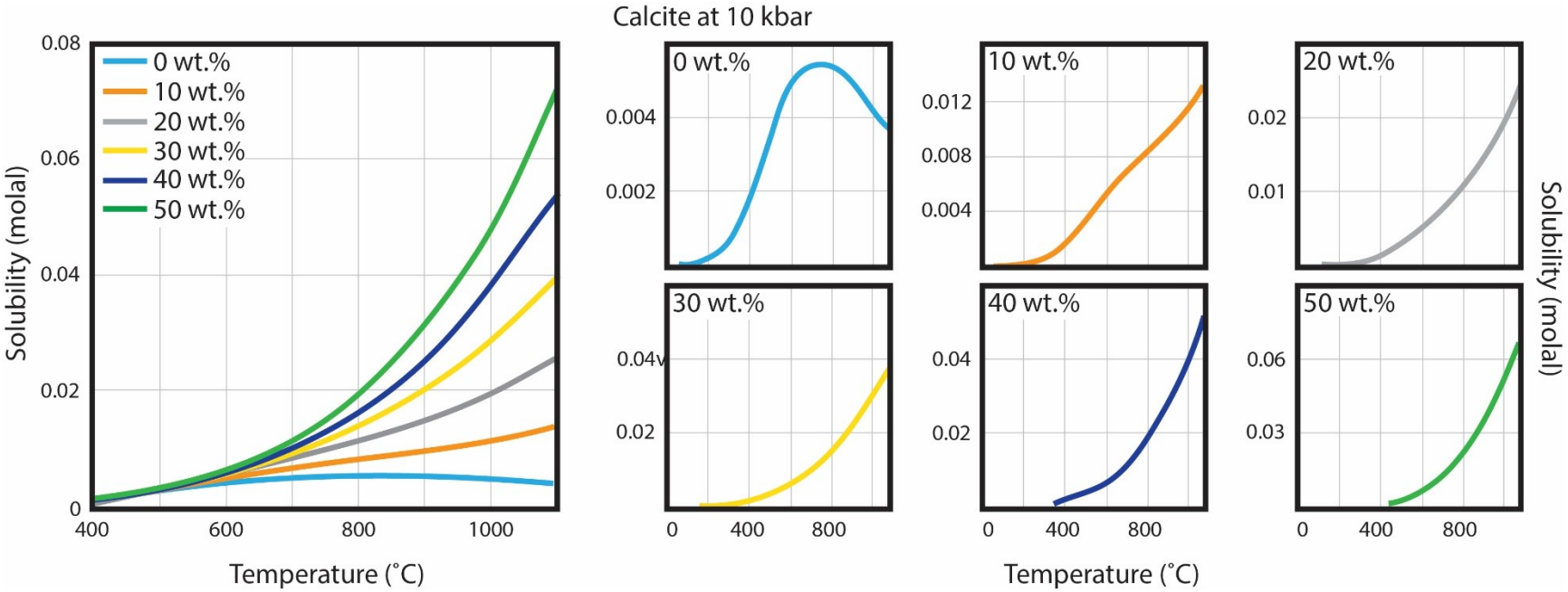

Figure 11: *T-x* diagram illustrating the effect of temperature and salinity on calcite solubility in H_2O±NaCl fluids at 10 kbar. A clear salting-in behavior is visible, with solubility increases progressively with increasing salinity. Retrograde solubility trends are seen at pure H_2O conditions, more gradual than those observed at lower pressures, and grading to prograde by ~20 wt.% NaCl salinity.

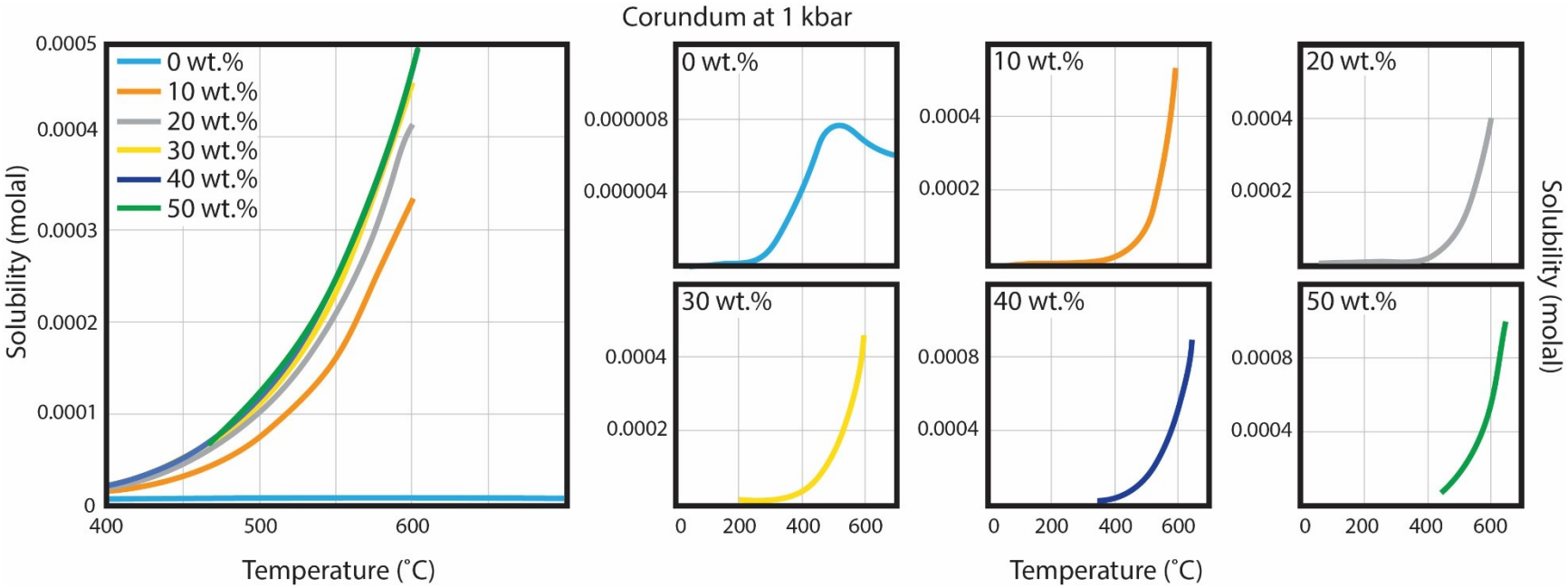

Figure 12: *T-x* diagram illustrating the effect of temperature and salinity on corundum solubility in H_2O±NaCl fluids at 1 kbar. Recall that due to limited experimental data on corundum solubility data in H_2O±NaCl fluids, trends in model predictions other than pure H_2O should be treated with caution. In pure H_2O, a retrograde solubility curve occurs at higher temperature conditions. The model predicts salting-in trends at 1 kbar.

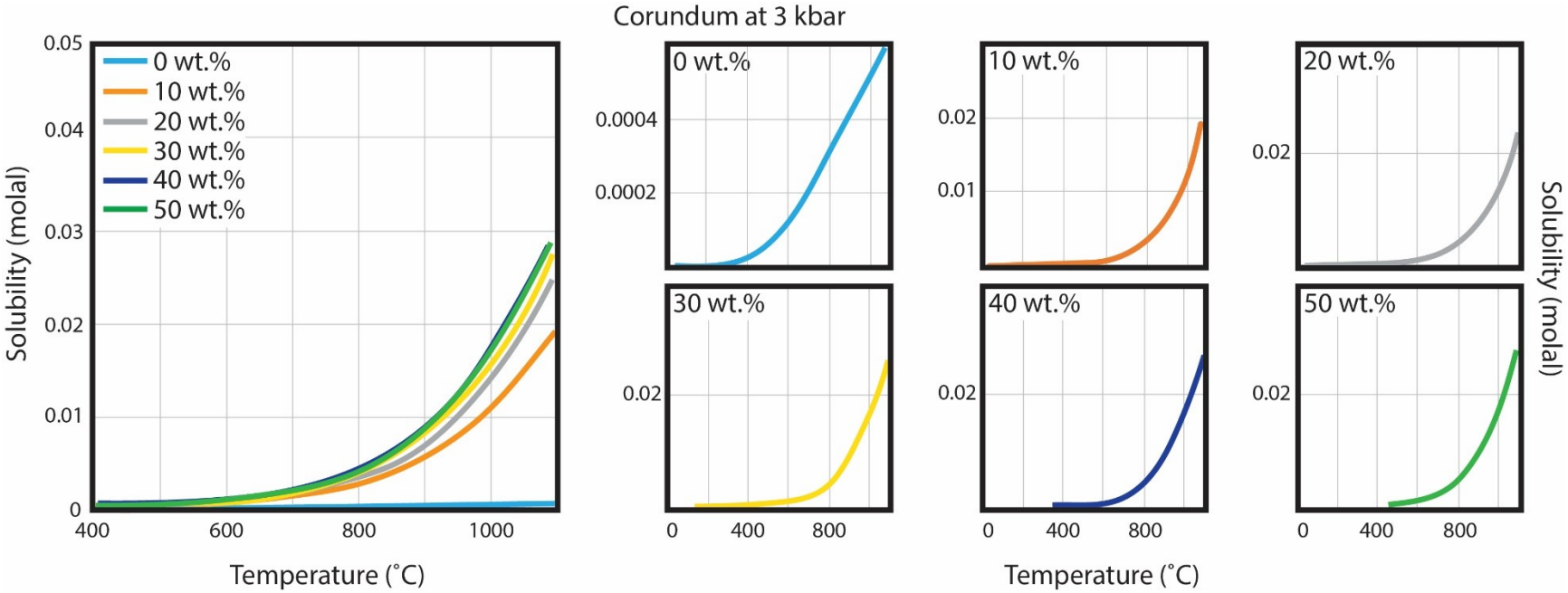

Figure 13: *T-x* diagram illustrating the effect of temperature and salinity on corundum solubility in H_2O±NaCl fluids at 3 kbar. Recall that due to limited experimental data on corundum solubility data in H_2O±NaCl fluids, trends in model predictions other than pure H_2O should be treated with caution. The model predicts salting-in trends at 3 kbar.

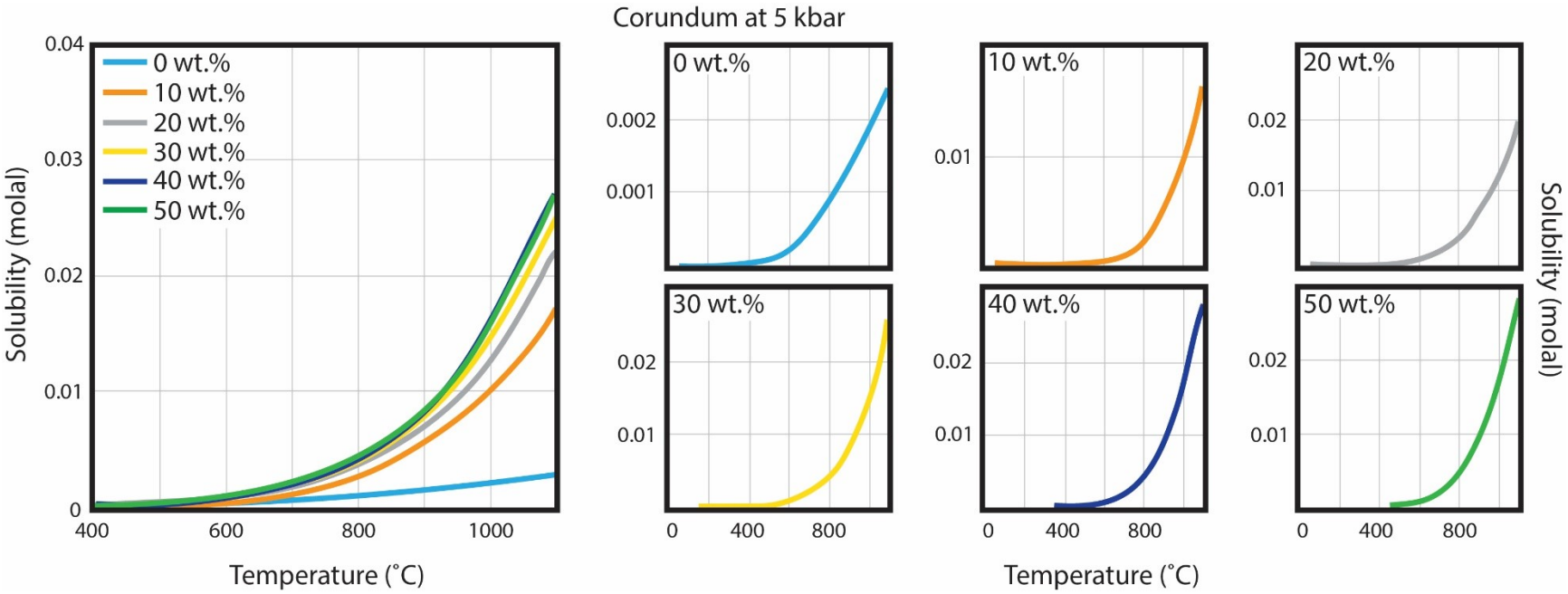

Figure 14: *T-x* diagram illustrating the effect of temperature and salinity on corundum solubility in H_2O±NaCl fluids at 5 kbar. Recall that due to limited experimental data on corundum solubility data in H_2O±NaCl fluids, trends in model predictions other than pure H_2O should be treated with caution. The model predicts salting-in trends at 5 kbar.

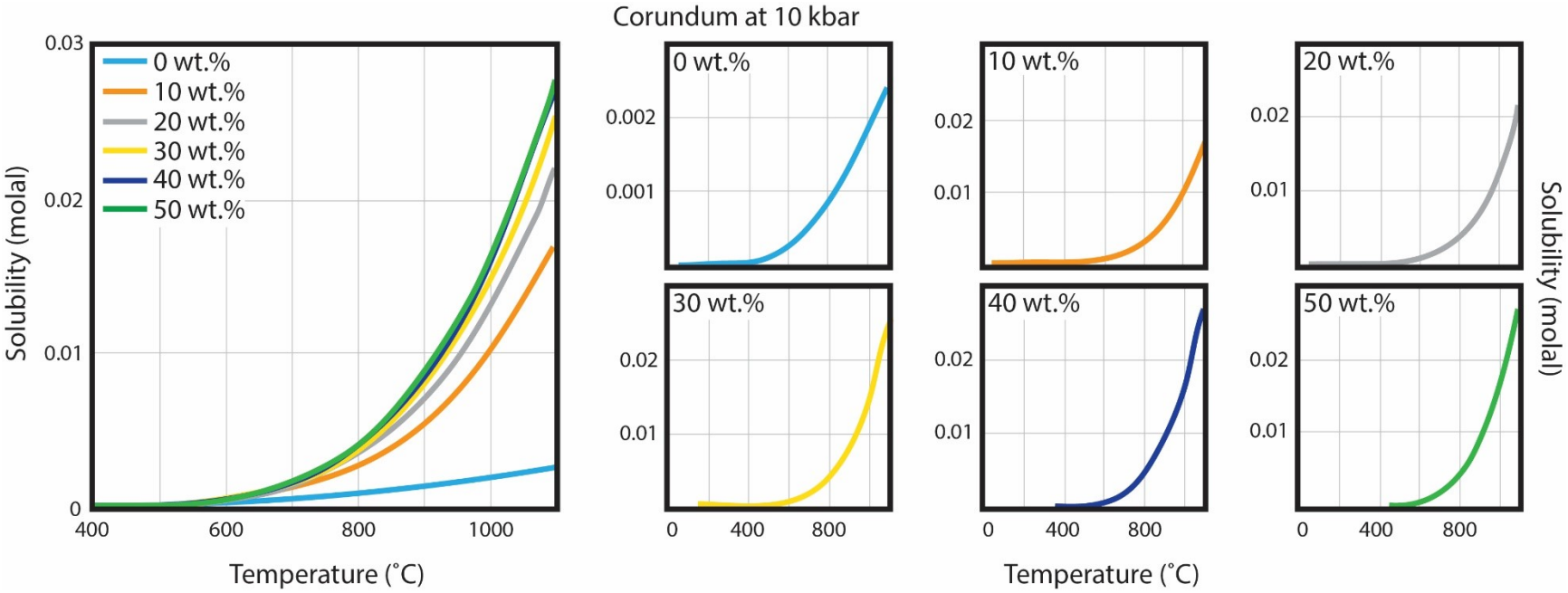

Figure 15: *T-x* diagram illustrating the effect of temperature and salinity on corundum solubility in H_2O±NaCl fluids at 10 kbar. Recall that due to limited experimental data on corundum solubility data in H_2O-NaCl fluids, trends in model predictions other than pure H_2O should be treated with caution. However, all regressed data points for Al_2O_3-H_2O±NaCl are at 800°C and 10 kbar, providing heightened constraint to this *T-x* diagram. Retrograde solubility trends seen in pure H_2O at low pressure have been replaced at 10 kbar by a fully prograde solubility trend. The model continues to the predict salting-in trends similarly to other pressures.

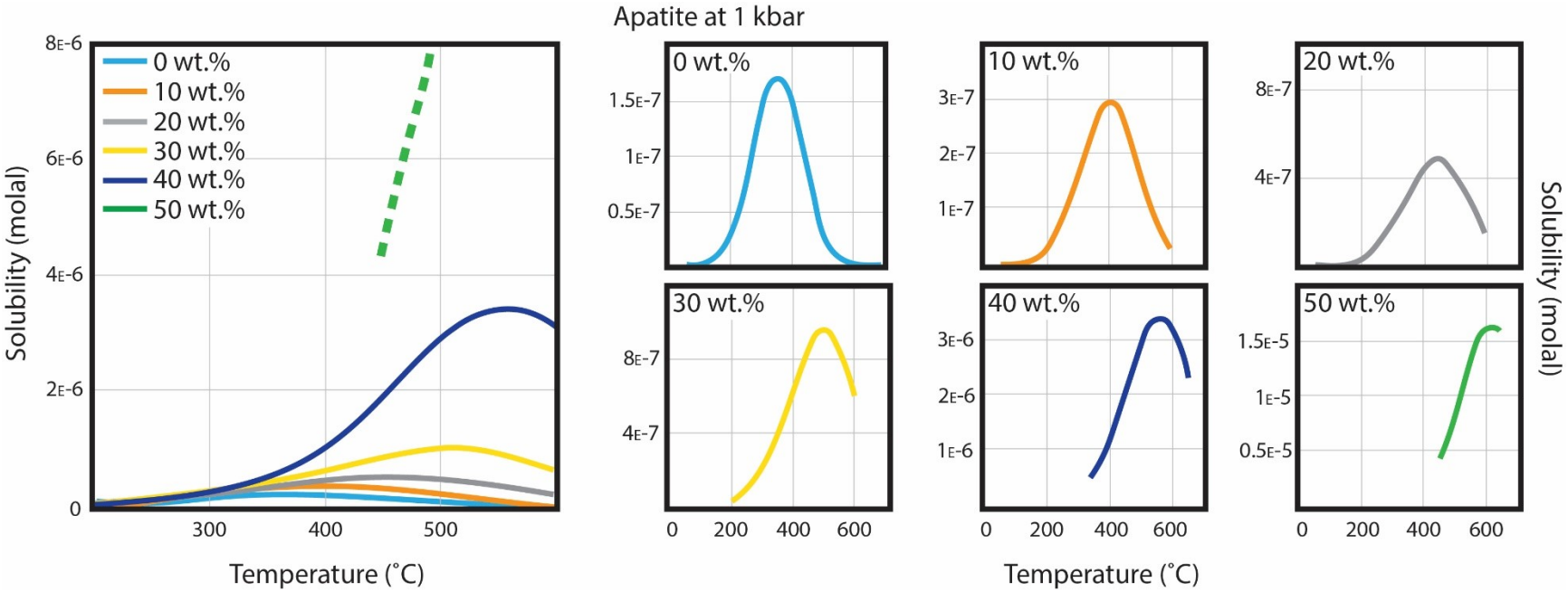

Figure 16: *T-x* diagram illustrating the effect of temperature and salinity on apatite solubility in H_2O±NaCl fluids at 1 kbar. Solubility generally increases progressively with increasing salinity. Salting-in and retrograde solubility behaviors are present for all *P-T-x* conditions. With increasing salinity, the peak of the retrograde curve shifts to increasingly higher temperatures. A large jump in predicted solubility at 50 wt.% NaCl salinity is shown here as dashed curve continuing off the figure to higher solubility.

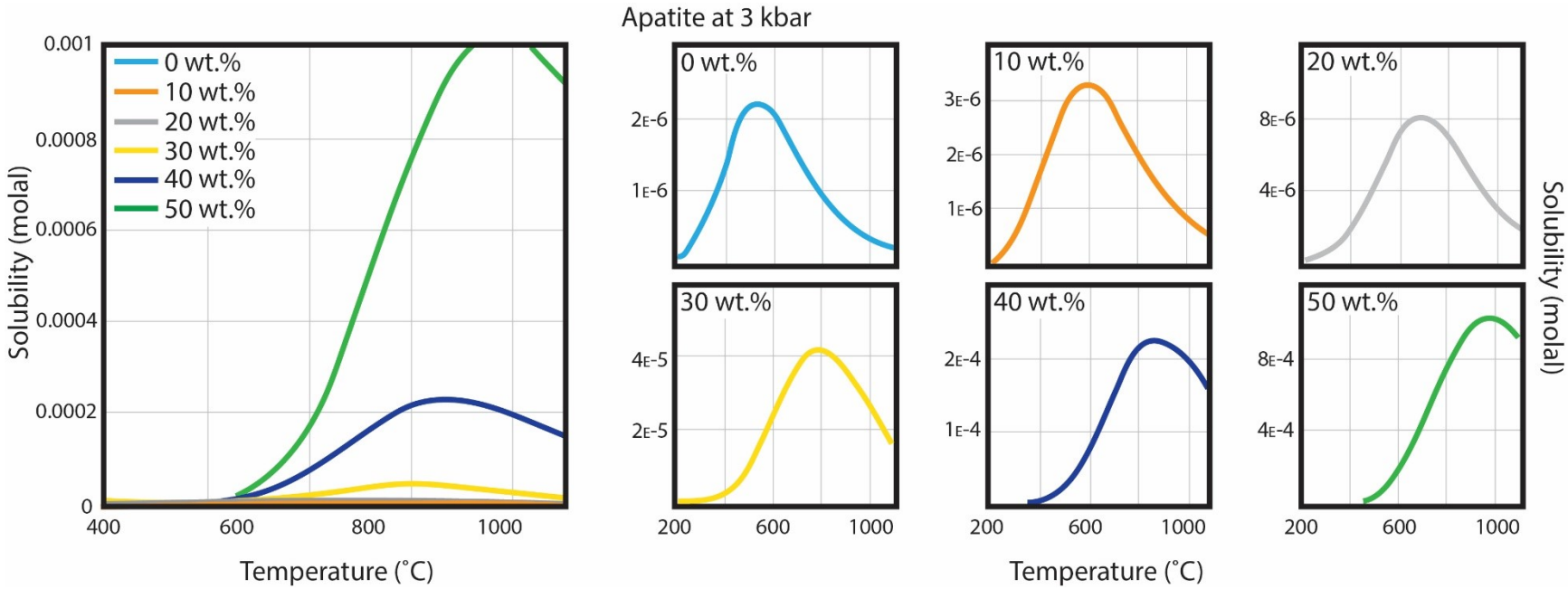

Figure 17: *T-x* diagram illustrating the effect of temperature and salinity on apatite solubility in H_2O±NaCl fluids at 3 kbar. Solubility increases with increasing salinity. Retrograde solubility trends are present at all salinity conditions, with peaks shifting to higher temperature at higher salinities.

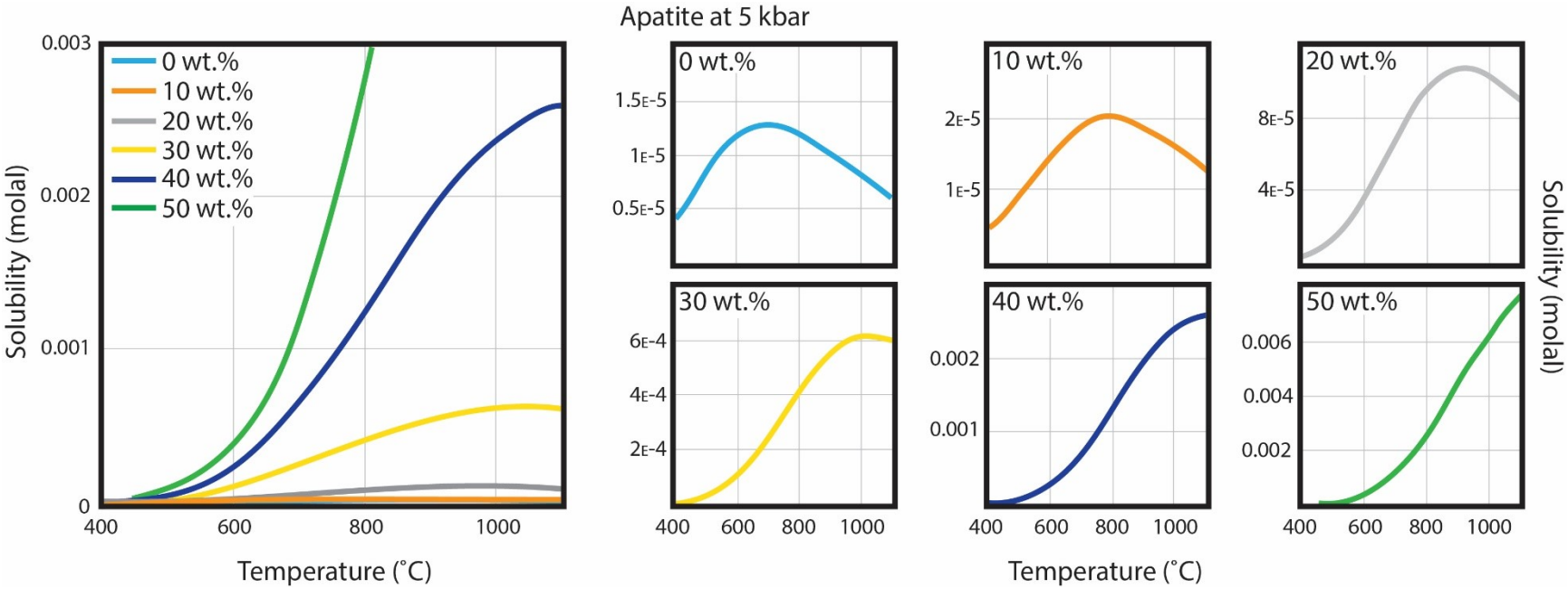

Figure 18: *T-x* diagram illustrating the effect of temperature and salinity on apatite solubility in H_2O±NaCl fluids at 5 kbar. Similarly to 1 kbar conditions, solubility increases with increasing salinity. Retrograde solubility curves are present at all salinity conditions, however, the parabolas cover such a wide range of temperature at these pressure conditions that we only see a small section of the curve. With increasing salinity, the peak of the retrograde curve shifts to increasingly higher temperatures. Solubility is significantly higher – 3 orders of magnitude – than apatite solubility at 1 kbar.

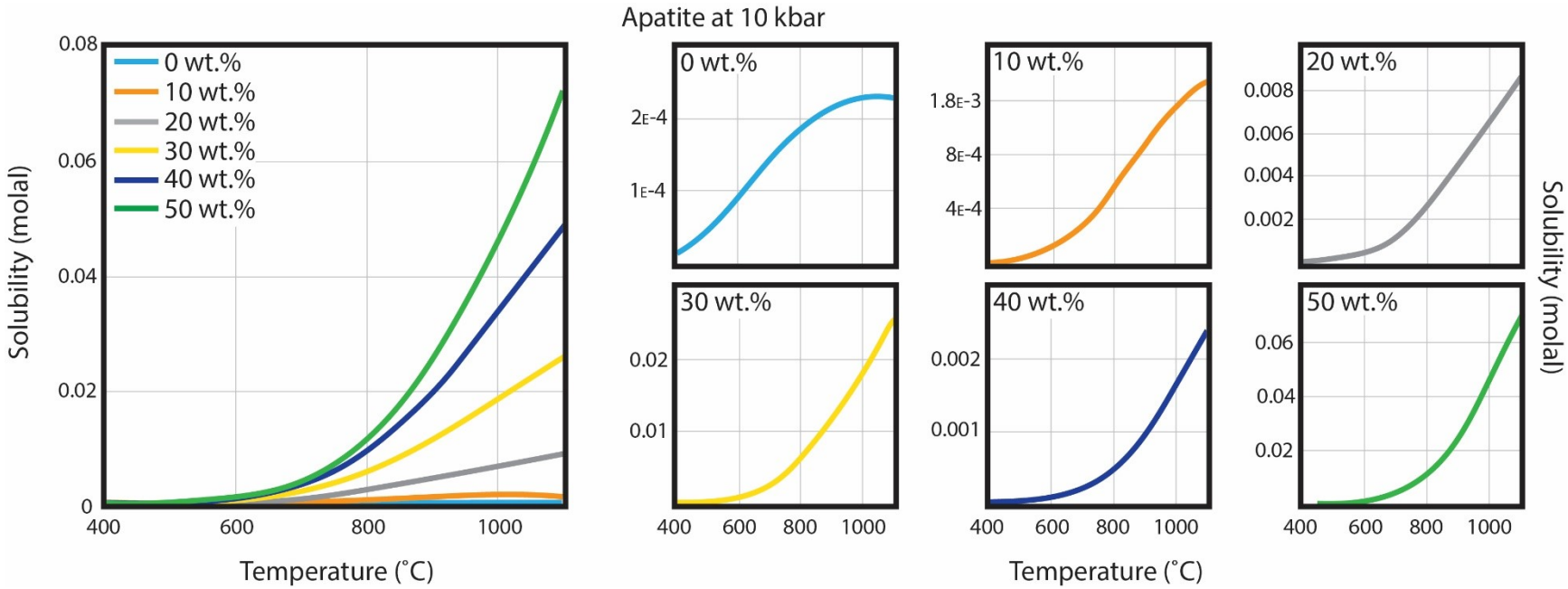

Figure 19: *T-x* diagram illustrating the effect of temperature and salinity on apatite solubility in H_2O±NaCl fluids at 10 kbar. Similarly to 3 kbar conditions, solubility increases with increasing salinity. Retrograde solubility curves are present at all salinity conditions, however, the parabolas cover such a wide range of temperature at these pressure conditions that we only see a small section of the curve. Solubility is significantly higher – 2 orders of magnitude – than apatite solubility at 3 kbar.

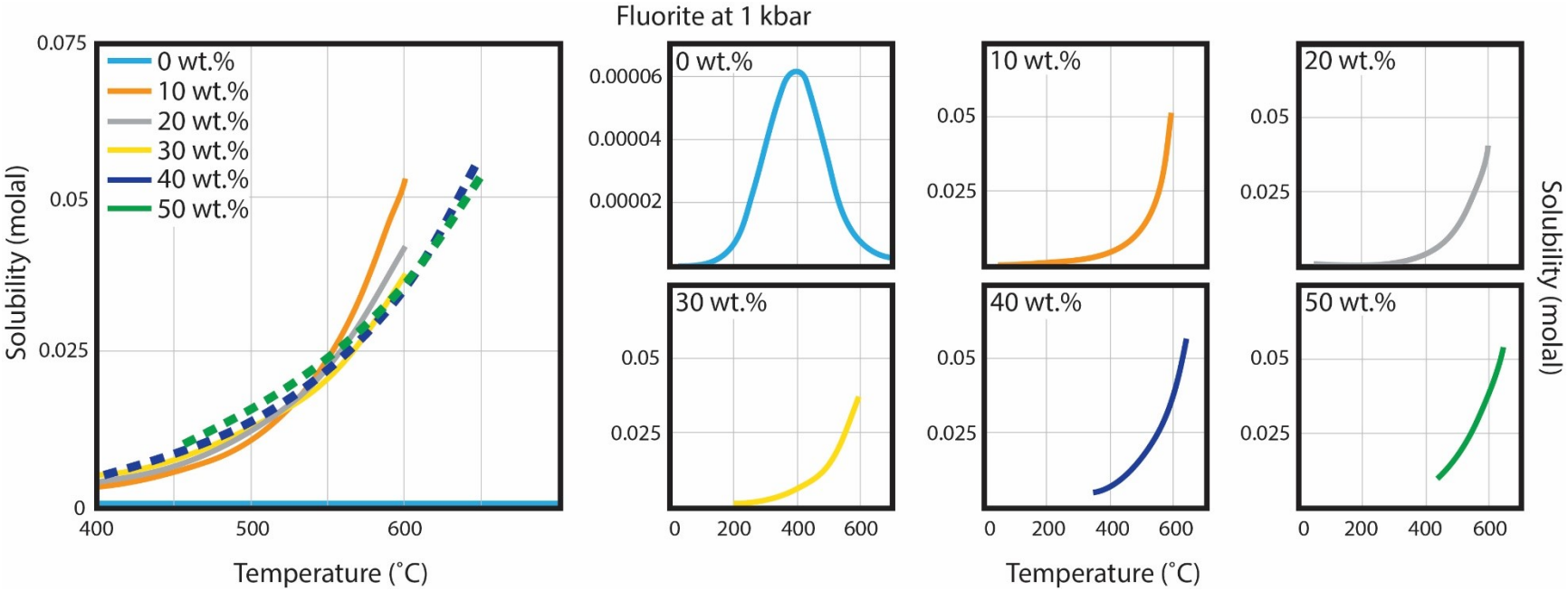

Figure 20: *T-x* diagram illustrating the effect of temperature and salinity on fluorite solubility in H_2O±NaCl fluids at 1 kbar. Solubility generally increases progressively with increasing salinity. Recall that due to limited experimental data on fluorite solubility data in H_2O-NaCl fluids, trends in model predictions other than pure H_2O should be treated with caution. In pure H_2O, a retrograde solubility trend is evidenced, quickly replaced by prograde solubility trends at salinities greater than dilute H_2O.

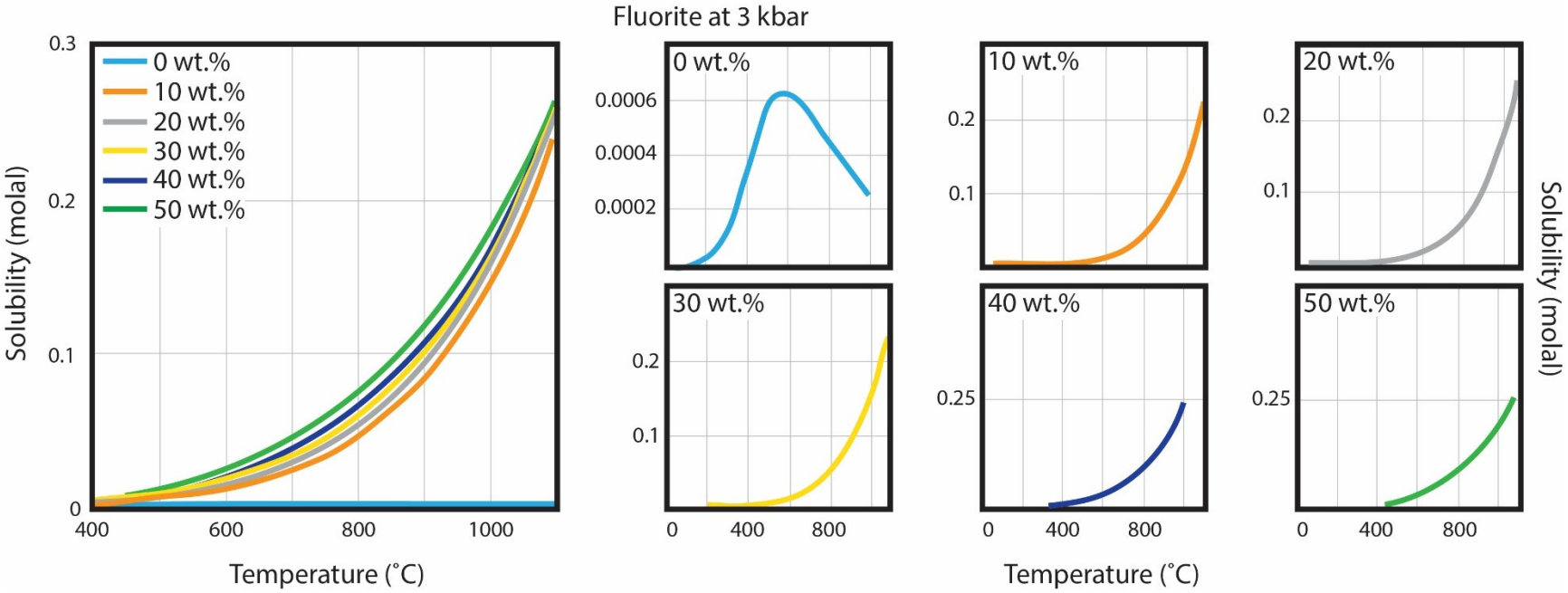

Figure 21: *T-x* diagram illustrating the effect of temperature and salinity on fluorite solubility in H_2O±NaCl fluids at 3 kbar. Solubility increases progressively with increasing salinity. Recall that due to limited experimental data on fluorite solubility data in H_2O-NaCl fluids, trends in model predictions other than pure H_2O should be treated with caution. In pure H_2O a retrograde solubility trend dominates, quickly replaced by prograde solubility trends at salinities greater than dilute H_2O.

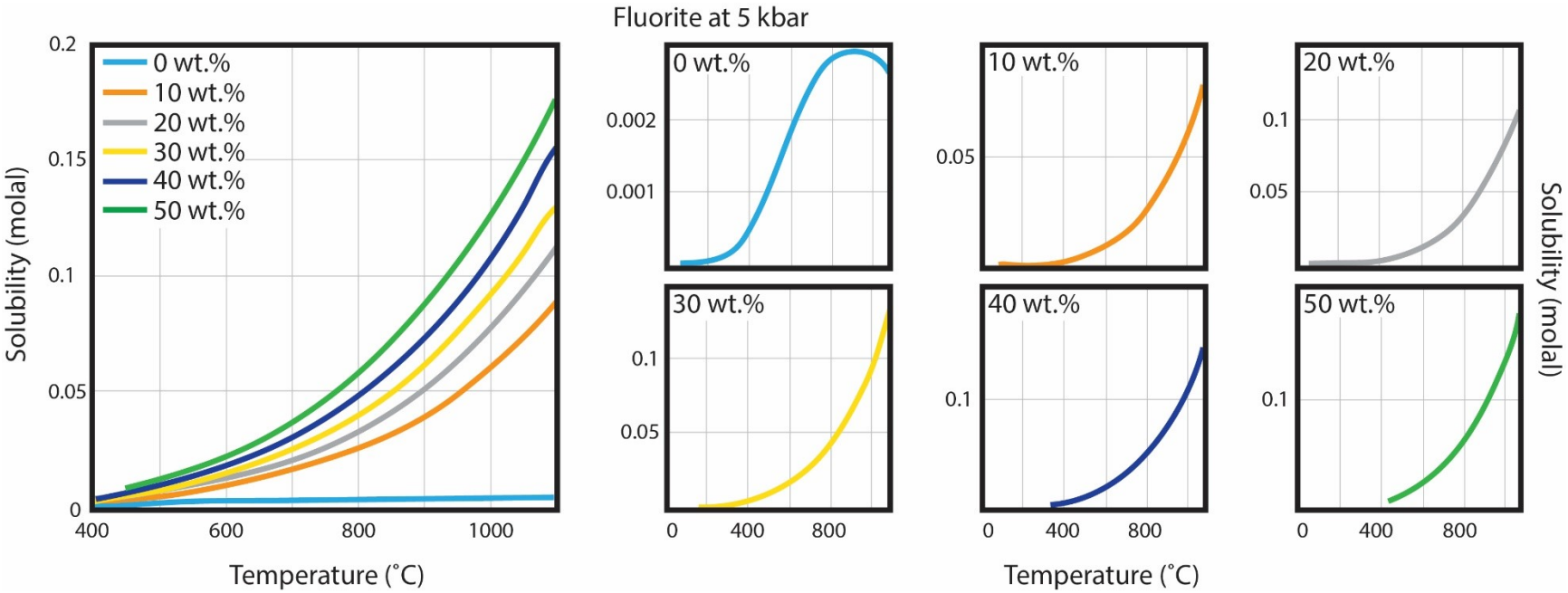

Figure 22: *T-x* diagram illustrating the effect of temperature and salinity on fluorite solubility in H_2O±NaCl fluids at 5 kbar. Recall that due to limited experimental data on fluorite solubility data in H_2O-NaCl fluids, trends in model predictions other than pure H_2O should be treated with caution. Retrograde solubility trends seen in pure H_2O at low pressure are more gradual than at 3 kbar. The model predicts salting-in trends.

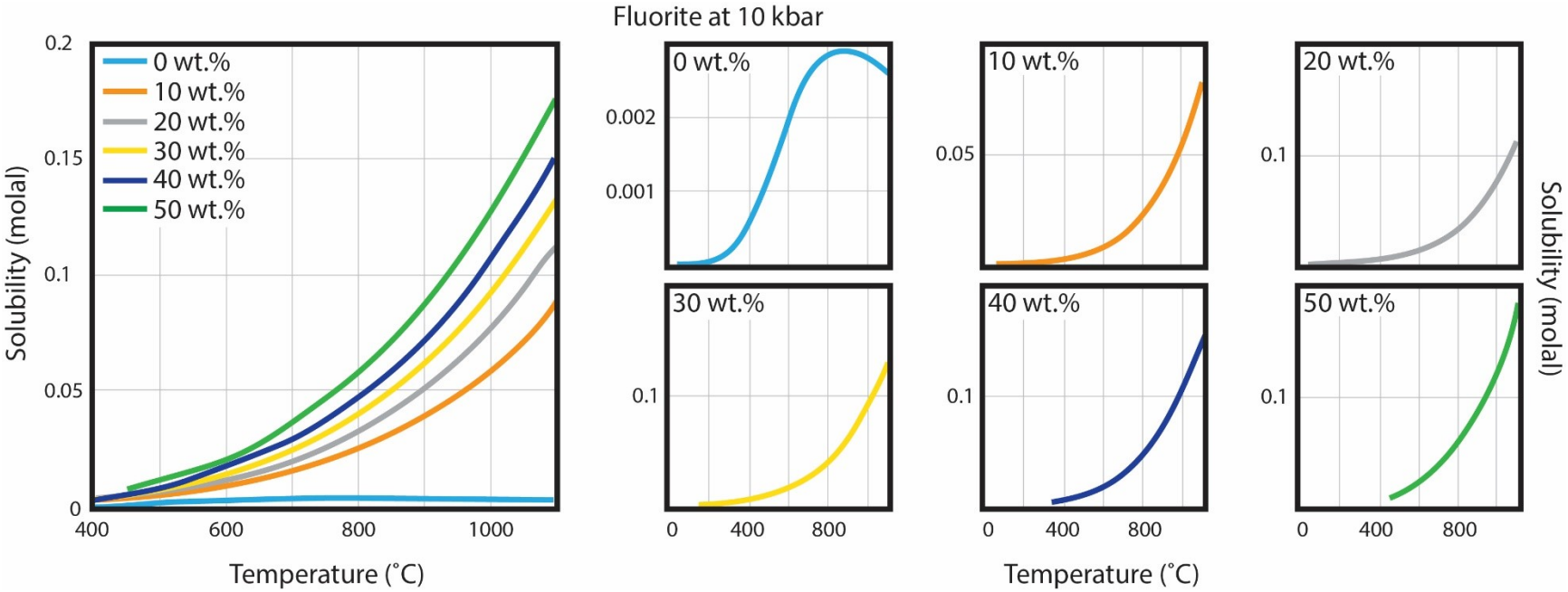

Figure 23: *T-x* diagram illustrating the effect of temperature and salinity on fluorite solubility in H_2O±NaCl fluids at 10 kbar. Recall that due to limited experimental data on fluorite solubility data in H_2O-NaCl fluids, trends in model predictions other than pure H_2O should be treated with caution. All four data points for CaF_3-H_2O±NaCl are at 800°C and 10 kbar, providing some constraint to this *T-x* diagram. Retrograde solubility trends seen in pure H_2O at low pressure are more gradual at 10 kbar. The model predicts salting-in trends.

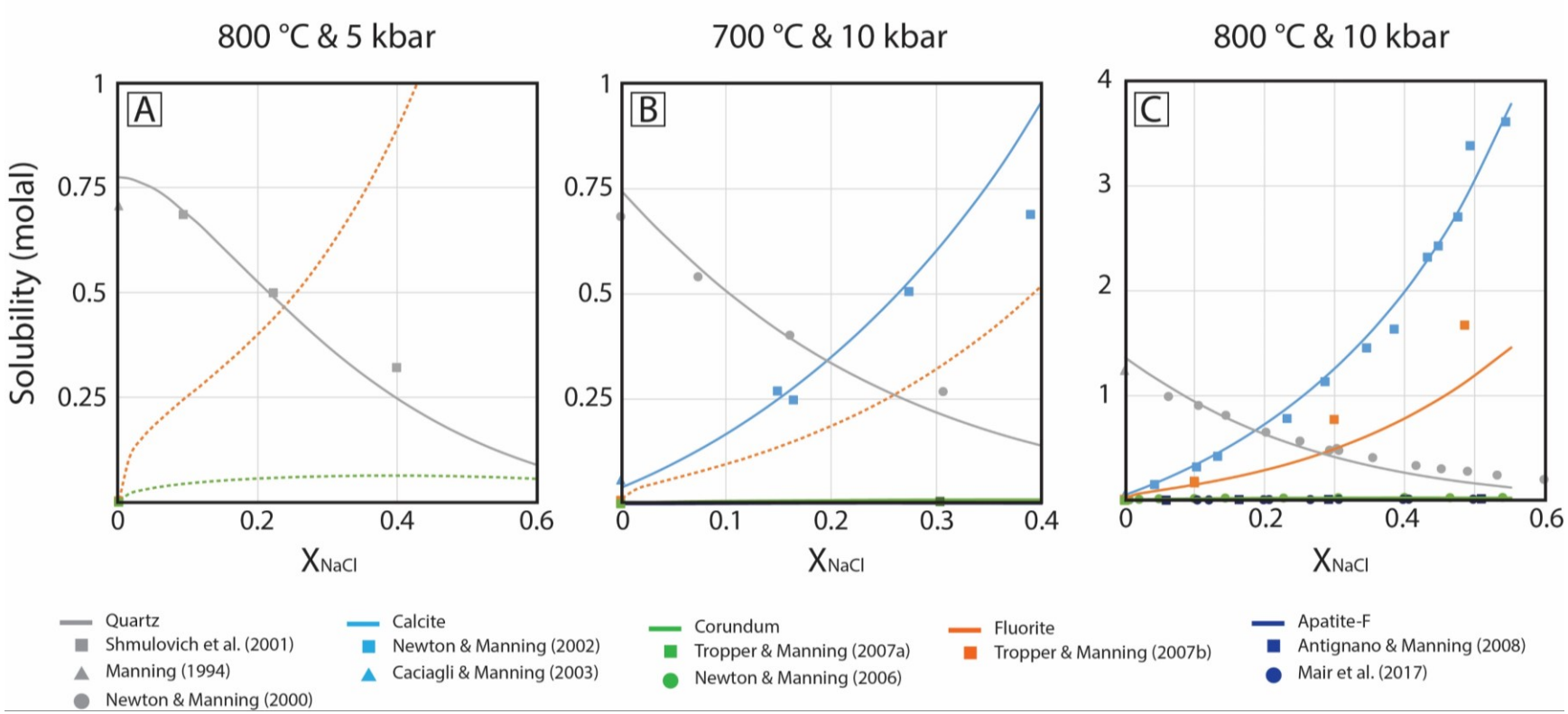

Figure 24 A-C: Mineral solubility in H_2O-NaCl fluids at selected *P-T* points. Density model predictions from this study are shown with continuous curves; solid where well constrained with experimental data and dashed where extrapolated. Symbols indicate experimental data at the specified conditions, colored to match the mineral dissolving.

REFERENCES

Akinfiev, N. N., and Diamond, L. W. (2009). A simple predictive model of quartz solubility in water–salt–CO_2 systems at temperatures up to 1000 C and pressures up to 1000 MPa. *Geochimica et Cosmochimica Acta*, *73*(6), 1597-1608.

Akinfiev, N., and Zotov, A. (1999). Thermodynamic description of equilibria in mixed fluids (H_2O-non-polar gas) over a wide range of temperature (25–700 C) and pressure (1–5000 bars). *Geochimica et Cosmochimica Acta*, *63*(13-14), 2025-2041

Alvarez, J., Corti, H. R., Fernández-Prini, R., and Japas, M. L. (1994). Distribution of solutes between coexisting steam and water. *Geochimica et Cosmochimica Acta*, *58*(13), 2789-2798.

Anderson, G. M., and Burnham, C. W. (1983). Feldspar solubility and the transport of aluminum under metamorphic conditions. *American Journal of Science*, 283, 283-297.

Andersen, T., and Neumann, E. R. (2001). Fluid inclusions in mantle xenoliths. *Lithos*, 55(1), 301-320.

Antignano, A., and Manning, C. E. (2008). Fluorapatite solubility in H_2O and H_2O–NaCl at 700 to 900°C and 0.7 to 2.0 GPa. *Chemical Geology*, *251*(1-4), 112-119.

Aranovich, L. Y., and Newton, R. C. (1996). H_2O activity in concentrated NaCl solutions at high pressures and temperatures measured by the brucite-periclase equilibrium. *Contributions to Mineralogy and Petrology*, *125*(2), 200-21.

Audétat, A., and Keppler, H. (2005). Solubility of rutile in subduction zone fluids, as determined by experiments in the hydrothermal diamond anvil cell. *Earth and Planetary Science Letters*, *232*(3-4), 393-402.

Ayers, J. C., and Watson, E. B. (1991). Solubility of apatite, monazite, zircon, and rutile in supercritical aqueous fluids with implications for subduction zone geochemistry. *Phil. Trans. R. Soc. Lond. A*, *335*(1638), 365-375.

Becker, K. H., Cemič, L., and Langer, K. E. (1983). Solubility of corundum in supercritical water. *Geochimica et Cosmochimica Acta*, *47*(9), 1573-1578.

Bischoff, J. L., Rosenbauer, R. J., and Pitzer, K. S. (1986). The system NaCl-H_2O: Relations of vapor-liquid near the critical temperature of water and of vapor-liquid-halite from 300 to 500°C. *Geochimica et Cosmochimica Acta*, *50*(7), 1437-1444.

Bodnar, R. J. (1983). A method of calculating fluid inclusion volumes based on vapor bubble diameters and PVTX properties of inclusion fluids. *Economic Geology*, *78*(3), 535-542.

Bodnar, R. J. (2003). Introduction to aqueous-electrolyte fluid inclusions. *Fluid inclusions: analysis and interpretation*, *32*, 81-100.

Bodnar, R. J., and Vityk M. O. (1994). Interpretation of microthermometric data for H_2O-NaCl fluid inclusions. *in* Fluid Inclusions in Minerals, Methods and Applications, B. De Vivo and M. L. Frezzotti, eds., published by Virginia Tech, Blacksburg, VA, p. 117-130.

Bodnar, R. J., Lecumberri-Sanchez, P., Moncada, D., and Steele-MacInnis, M. (2014). 13.5—Fluid inclusions in hydrothermal ore deposits. *Treatise on Geochemistry, Second Editionth edn. Elsevier, Oxford*, 119-142.

Borg, R. J., and Dienes, G. J. (1992). The physical chemistry of solids. Academic Press.

Born, M. (1920). Volumen und hydratationswärme der ionen. *Zeitschrift für Physik*, *1*(1), 45-48.

Bowers, T. S., and Helgeson, H. C. (1983). Calculation of the thermodynamic and geochemical consequences of nonideal mixing in the system H_2O-CO_2-NaCl on phase relations in geologic systems: Equation of state for H_2O-CO_2-NaCl fluids at high pressures and temperatures. *Geochimica et Cosmochimica Acta*, *47*(7), 1247-1275.

Caciagli, N. C., and Manning, C. E. (2003). The solubility of calcite in water at 6–16 kbar and 500–800°C. *Contributions to Mineralogy and Petrology*, *146*(3), 275-285.

Cathles III, L. M. (1990). Scales and effects of fluid flow in the upper crust. *Science*, *248*(4953), 323-330.

Cruz, M. F., and Manning, C. E. (2015). Experimental determination of quartz solubility and melting in the system SiO_2–H_2O–NaCl at 15–20 kbar and 900–1100°C: implications for silica polymerization and the formation of supercritical fluids. *Contributions to Mineralogy and Petrology*, *170*(4), 35.

Dolejš, D., and Manning, C. E. (2010). Thermodynamic model for mineral solubility in aqueous fluids: theory, calibration and application to model fluid-flow systems. *Geofluids*, *10*(1-2), 20-40.

Driesner, T. (2007). The system H_2O–NaCl. Part II: Correlations for molar volume, enthalpy, and isobaric heat capacity from 0 to 1000°C, 1 to 5000bar, and 0 to 1 X NaCl. *Geochimica et Cosmochimica Acta*, *71*(20), 4902-4919.

Dubé, B., and Gosselin, P. (2007). Greenstone-hosted quartz-carbonate vein deposits. *Mineral Deposits of Canada: A synthesis of major deposit-types, district metallogeny, the evolution of geological provinces, and exploration methods: Geological Association of Canada, Mineral Deposits Division, Special Publication*, *5*, 49-73.

Emsbo, P., Seal, R. R., Breit, G. N., Diehl, S. F., and Shah, A. K. (2016). *Sedimentary exhalative (sedex) zinc-lead-silver deposit model* (No. 2010-5070-N). US Geological Survey.

Fein, J. B., and Walther, J. V. (1989). Calcite solubility and speciation in supercritical NaCl-HCl aqueous fluids. *Contributions to Mineralogy and Petrology*, *103*(3), 317-324.

Fournier, R. O., and Marshall, W. L. (1983). Calculation of amorphous silica solubilities at 25 to 300 C and apparent cation hydration numbers in aqueous salt solutions using the concept of effective density of water. *Geochimica et Cosmochimica Acta*, *47*(3), 587-596.

Fritz, P., and Frape, S. T. (1982). Saline groundwaters in the Canadian Shield—a first overview. *Chemical Geology*, *36*(1-2), 179-190.

Frezzotti, M. L. (2001). Silicate-melt inclusions in magmatic rocks: applications to petrology. *Lithos*, *55*(1), 273-299.

Galvez, M. E., Manning, C. E., Connolly, J. A., and Rumble, D. (2015). The solubility of rocks in metamorphic fluids: A model for rock-dominated conditions to upper mantle pressure and temperature. *Earth and Planetary Science Letters*, *430*, 486-498.

Gao, J., John, T., Klemd, R., and Xiong, X. (2007). Mobilization of Ti–Nb–Ta during subduction: evidence from rutile-bearing dehydration segregations and veins hosted in eclogite, Tianshan, NW China. *Geochimica et Cosmochimica Acta*, *71*(20), 4974-4996.

Goldstein, R. H. (2001). Fluid inclusions in sedimentary and diagenetic systems. *Lithos*, *55*(1), 159-193.

Groves, D. I., Bierlein, F. P., Meinert, L. D., and Hitzman, M. W. (2010). Iron oxide copper-gold (IOCG) deposits through Earth history: Implications for origin, lithospheric setting, and distinction from other epigenetic iron oxide deposits. *Economic Geology*, *105*(3), 641-654.

Hanor, J. S. (1994). Origin of saline fluids in sedimentary basins. *Geological Society, London, Special Publications*, *78*(1), 151-174.

Harvey, A. H., and Levelt Sengers, J. M. H. (1990). Correlation of aqueous Henry's constants from 0° C to the critical point. *AIChE journal*, *36*(4), 539-546.

Hashimoto, A. (1992). The effect of H_2O gas on volatilities of planet-forming major elements: I. Experimental determination of thermodynamic properties of Ca-, Al-, and Si-hydroxide gas molecules and its application to the solar nebula. *Geochimica et Cosmochimica Acta*, 56(1), 511-532.

Hedenquist, J. W., and Lowenstern, J. B. (1994). The role of magmas in the formation of hydrothermal ore deposits. *Nature*, *370*(6490), 519.

Helgeson, H. C., Kirkham, D. H., and Flowers, G. C. (1981). Theoretical prediction of the thermodynamic behavior of aqueous electrolytes by high pressures and temperatures; IV, Calculation of activity coefficients, osmotic coefficients, and apparent molal and standard and relative partial molal properties to 600 degrees C and 5kb. *American Journal of Science*, *281*(10), 1249-1516.

Helgeson, H. C., and Kirkham, D. H. (1976). Theoretical prediction of thermodynamic properties of aqueous electrolytes at high pressures and temperatures. III. Equation of state for aqueous species at infinite dilution. *American Journal of Science*, *276*(2).

Hemley, J. J., Montoya, J. W., Marinenko, J. W., and Luce, R. W. (1980). Equilibria in the system Al_2O_3-SiO_2-H_2O and some general implications for alteration/mineralization processes. *Economic Geology*, *75*(2), 210-228.

Hunt, J. D., and Manning, C. E. (2012). A thermodynamic model for the system SiO_2–H2O near the upper critical end point based on quartz solubility experiments at 500–1100°C and 5–20 kbar. *Geochimica et Cosmochimica Acta*, *86*, 196-213.

Hunt, J. D., Kavner, A., Schauble, E. A., Snyder, D., and Manning, C. E. (2011). Polymerization of aqueous silica in H2O–K2O solutions at 25–200°C and 1 bar to 20 kbar. *Chemical Geology*, *283*(3-4), 161-170.

Kennedy, G. C. (1950). A portion of the system silica-water. *Economic Geology*, *45*(7), 629-653.

Kebarle, P. (1977). Ion thermochemistry and solvation from gas phase ion equilibria. *Annual Review of Physical Chemistry*, 28(1), 445-476.

Kesler, S. E. (2005). Ore-forming fluids. *Elements*, *1*(1), 13-18.

Lecumberri-Sanchez, P., Steele-MacInnis, M., and Bodnar, R. J. (2012). A numerical model to estimate trapping conditions of fluid inclusions that homogenize by halite disappearance. *Geochimica et Cosmochimica Acta*, *92*, 14-22.

Mair, P., Tropper, P., Harlov, D. E., and Manning, C. E. (2017). The solubility of apatite in H_2O, KCl-H_2O, NaCl-H_2O at 800°C and 1.0 GPa: Implications for REE mobility in high-grade saline brines. *Chemical Geology*, *470*, 180-192.

Manning, C. E. (1994). The solubility of quartz in H_2O in the lower crust and upper mantle. *Geochimica et Cosmochimica Acta*, *58*(22), 4831-4839.

Manning, C. E. (2004). The chemistry of subduction-zone fluids. *Earth and Planetary Science Letters*, *223*(1), 1-16.

Manning, C. E., Shock, E. L., and Sverjensky, D. A. (2013). The chemistry of carbon in aqueous fluids at crustal and upper-mantle conditions: experimental and theoretical constraints. *Reviews in Mineralogy and Geochemistry*, *75*(1), 109-148.

Marshall, W. L. (2008). Dielectric constant of water discovered to be simple function of density over extreme ranges from –35 to +600°C and to 1200 MPa (12000 atm.), believed universal. *Nature Preceedings.* doi:10.1038/npre.2008.2472.1

Marshall, W. L., and Franck, E. U. (1981). Ion product of water substance, 0–1000°C, 1–10,000 bars new international formulation and its background. *Journal of physical and chemical reference data*, *10*(2), 295-304.

Marshall, W. L., and Quist, A. S. (1967). A representation of isothermal ion-ion-pair-solvent equilibria independent of changes in dielectric constant. *Proceedings of the National Academy of Sciences*, *58*(3), 901-906.

McKeag, S. A., and Craw, D. (1989). Contrasting fluids in gold-bearing quartz vein systems formed progressively in a rising metamorphic belt; Otago Schist, New Zealand. *Economic geology*, *84*(1), 22-33.

Mercier, A., Debat, P., and Saul, J. M. (1999). Exotic origin of the ruby deposits of the Mangari area in SE Kenya. *Ore Geology Reviews*, *14*(2), 83-104.

Morey, G. W. (1962). Action of water on calcite, magnesite and dolomite. *American Mineralogist*, *47*(11-1), 1456-1460.

Newton, R. C., and Manning, C. E. (2000). Quartz solubility in H_2O-NaCl and H_2O-CO_2 solutions at deep crust-upper mantle pressures and temperatures: 2–15 kbar and 500–900°C. *Geochimica et Cosmochimica Acta*, *64*(17), 2993-3005.

Newton, R. C., and Manning, C. E. (2002). Experimental determination of calcite solubility in H2O-NaCl solutions at deep crust/upper mantle pressures and temperatures: Implications for metasomatic processes in shear zones. *American Mineralogist*, *87*(10), 1401-1409.

Newton, R. C., and Manning, C. E. (2003). Activity coefficient and polymerization of aqueous silica at 800°C, 12 kbar, from solubility measurements on SiO_2-buffering mineral assemblages. *Contributions to Mineralogy and Petrology*, *146*(2), 135-143.

Newton, R. C., and Manning, C. E. (2006). Solubilities of corundum, wollastonite and quartz in H_2O–NaCl solutions at 800°C and 10kbar: interaction of simple minerals with brines at high pressure and temperature. *Geochimica et Cosmochimica Acta*, *70*(22), 5571-5582.

Newton, R. C., and Manning, C. E. (2008). Thermodynamics of SiO_2–H_2O fluid near the upper critical end point from quartz solubility measurements at 10 kbar. *Earth and Planetary Science Letters*, *274*(1), 241-249.

Newton, R. C., and Manning, C. E. (2010). Role of saline fluids in deep-crustal and upper-mantle metasomatism: insights from experimental studies. *Geofluids*, *10*(1-2), 58-72.

Palmer, D. A., Simonson, J. M., and Jensen, J. P. (2004). Partitioning of electrolytes to steam and their solubilities in steam. In *Aqueous Systems at Elevated Temperatures and Pressures* (pp. 409-439).

Philippot, P., and Selverstone, J. (1991). Trace-element-rich brines in eclogitic veins: implications for fluid composition and transport during subduction. *Contributions to Mineralogy and Petrology*, *106*(4), 417-430.

Pitzer, K. S. (1983). Thermodynamics of sodium chloride solutions in steam. *The Journal of Physical Chemistry*, 87(7), 1120-1125.

Putnis, A., and Austrheim, H. (2010). Fluid-induced processes: metasomatism and metamorphism. *Geofluids*, *10*(1-2), 254-269.

Ragnarsdóttir, K. V., and Walther, J. V. (1985). Experimental determination of corundum solubilities in pure water between 400–700°C and 1–3 kbar. *Geochimica et Cosmochimica Acta*, *49*(10), 2109-2115.

Rapp, J. F., Klemme, S., Butler, I. B., and Harley, S. L. (2010). Extremely high solubility of rutile in chloride and fluoride-bearing metamorphic fluids: An experimental investigation. *Geology*, *38*(4), 323-326.

Robert, F., Boullier, A. M., and Firdaous, K. (1995). Gold-quartz veins in metamorphic terranes and their bearing on the role of fluids in faulting. *Journal of Geophysical Research: Solid Earth*, *100*(B7), 12861-12879.

Roedder, E. (1971). Fluid inclusion studies on the porphyry-type ore deposits at Bingham, Utah, Butte, Montana, and Climax, Colorado. *Economic Geology*, *66*(1), 98-118.

Rosenbaum, J. M., Zindler, A., and Rubenstone, J. L. (1996). Mantle fluids: evidence from fluid inclusions. *Geochimica et Cosmochimica Acta*, 60(17), 3229-3252.

Rustad, J. R., and Hay, B. P. (1995). A molecular dynamics study of solvated orthosilicic acid and orthosilicate anion using parameterized potentials. *Geochimica et Cosmochimica Acta*, 59(7), 1251-1257.

Sakuma, H., and Ichiki, M. (2016). Density and isothermal compressibility of supercritical H_2O–NaCl fluid: molecular dynamics study from 673 to 2000 K, 0.2 to 2 GPa, and 0 to 22 wt% NaCl concentrations. *Geofluids*, 16(1), 89-102.

Schloemer, V. H. (1952). Hydrothermale untersuchungen über das System CaO-MgO-CO_2-H_2O. *Neus Jahrbuch für Mineralogie Monatshefte*, 1952,129-135.

Sefcik, J., and Goddard, W. A. (2001). Thermochemistry of silicic acid deprotonation: Comparison of gas-phase and solvated DFT calculations to experiment. *Geochimica et Cosmochimica Acta*, 65(24), 4435-4443.

Shmulovich, K., Graham, C., and Yardley, B. (2001). Quartz, albite and diopside solubilities in H_2O–NaCl and H_2O–CO_2 fluids at 0.5–0.9 GPa. *Contributions to Mineralogy and Petrology*, *141*(1), 95-108.

Shmulovich, K. I., Yardley, B. W. D., and Graham, C. M. (2006). Solubility of quartz in crustal fluids: experiments and general equations for salt solutions and H_2O–CO_2 mixtures at 400–800°C and 0.1–0.9 GPa. *Geofluids*, *6*(2), 154-167.

Shock, E. L., Helgeson, H. C., and Sverjensky, D. A. (1989). Calculation of the thermodynamic and transport properties of aqueous species at high pressures and temperatures: Standard partial molal properties of inorganic neutral species. *Geochimica et Cosmochimica Acta*, *53*(9), 2157-2183.

Spandler, C., and Pirard, C. (2013). Element recycling from subducting slabs to arc crust: A review. *Lithos*, *170*, 208-223.

Steele-MacInnis, M., and Bodnar, R. J. (2013). Effect of the vapor phase on the salinity of halite-bearing aqueous fluid inclusions estimated from the halite dissolution temperature. *Geochimica et Cosmochimica Acta*, *115*, 205-216.

Strübel, G. (1965). Quantitative Untersuchungen über die hydrothermale Löslichkeit von Flußspat (CaF_2). *Neues Jahrbuch für Mineralogie, Monatshefte*, *1965*, 83–95.

Touret, J. L. R. (2001). Fluids in metamorphic rocks. *Lithos*, *55*(1), 1-25.

Tropper, P., and Manning, C. E. (2007a). The solubility of corundum in H_2O at high pressure and temperature and its implications for Al mobility in the deep crust and upper mantle. *Chemical Geology*, *240*(1), 54-60.

Tropper, P., and Manning, C. E. (2007b). The solubility of fluorite in H_2O and H_2O–NaCl at high pressure and temperature. *Chemical Geology*, *242*(3-4), 299-306.

Walther, J. V. (1997). Experimental determination and interpretation of the solubility of corundum in H_2O between 350 and 600°C from 0.5 to 2.2 kbar. *Geochimica et Cosmochimica Acta*, *61*(23), 4955-4964.

Walther, J. V. (2001). Experimental determination and analysis of the solubility of corundum in 0.1 and 0.5 m NaCl solutions between 400 and 600°C from 0.5 to 2.0 kbar. *Geochimica et Cosmochimica Acta*, *65*(17), 2843-2851.

Walther, J. V., and Helgeson, H. C. (1977). Calculation of the thermodynamic properties of aqueous silica and the solubility of quartz and its polymorphs at high pressures and temperatures. *American Journal of Science 277*(10), 1315-1351.

Walther, J. V., and Long, M. I. (1986). Experimental determination of calcite solubilities in supercritical H2O. In: *Proceedings of the Fifth International Symposium on Water-Rock Interaction* (ed. Hitchon, R.B.), Vol. 5, pp. 609-611. National Energy Authority, Reykjavik, Iceland.

Walther, J. V., and Orville, P. M. (1983). The extraction-quench technique for determination of the thermodynamic properties of solute complexes: application to quartz solubility in fluid mixtures. *American Mineralogist*, *68*, 731-741.

Walter, B. F., Steele-MacInnis, M., and Markl G. (2017). Sulfate brines in fluid inclusions of hydrothermal veins: Compositional determinations in the system H_2O-Na-Ca-Cl-SO_4. *Geochimica et Cosmochimica Acta*, 209, 184-203.

Weis, P. (2015). The dynamic interplay between saline fluid flow and rock permeability in magmatic-hydrothermal systems. *Geofluids*, *15*(1-2), 350-371.

White, D. E. (1974). Diverse origins of hydrothermal ore fluids. *Economic Geology*, *69*(6), 954-973.

Wilkinson, J. J. (2001). Fluid inclusions in hydrothermal ore deposits. *Lithos*, *55*(1), 229-272.

Xie, Z., and Walther, J. V. (1993). Quartz solubilities in NaCl solutions with and without wollastonite at elevated temperatures and pressures. *Geochimica et Cosmochimica Acta*, *57*(9), 1947-1955.

Yardley, B. W. (2005). 100th Anniversary Special Paper: metal concentrations in crustal fluids and their relationship to ore formation. *Economic Geology*, *100*(4), 613-632.

Yardley, B. W. D., and Graham, J. T. (2002). The origins of salinity in metamorphic fluids. *Geofluids*, *2*(4), 249-256.

Zotov, N., and Keppler, H. (2002). Silica speciation in aqueous fluids at high pressures and high temperatures. *Chemical Geology*, *184*(1), 71-78.

APPENDIX A

Supplemental Table 1: Quartz Data Base for Experimental Data of Mineral Solubility in H_2O-NaCl Fluids

Wt.% NaCl	T (°C)	P (bars)	ρ* (g/cm^3)	Source	Notes
14.61983	1000	15000	0.88855287	Cruz & Manning, 2015	
26.23253	1000	15000	0.87328561	Cruz & Manning, 2015	
26.52552	900	15000	0.8971942	Cruz & Manning, 2015	
45.79078	1000	15000	0.80415606	Cruz & Manning, 2015	
57.82039	1050	15000	0.74318906	Cruz & Manning, 2015	
58.17843	1080	15000	0.73905512	Cruz & Manning, 2015	
58.18042	1000	20000	0.75897057	Cruz & Manning, 2015	
58.22128	1000	15000	0.7452046	Cruz & Manning, 2015	
58.22875	1090	15000	0.73803488	Cruz & Manning, 2015	
58.55119	950	15000	0.74771722	Cruz & Manning, 2015	
58.57189	1000	15000	0.74339937	Cruz & Manning, 2015	
67.11894	1000	15000	0.69834377	Cruz & Manning, 2015	
67.96935	1050	15000	0.69067643	Cruz & Manning, 2015	
76.18542	1100	15000	0.64515579	Cruz & Manning, 2015	
76.40943	900	15000	0.65452013	Cruz & Manning, 2015	
76.45485	1000	20000		Cruz & Manning, 2015	L+H
76.63013	1050	15000	0.64519558	Cruz & Manning, 2015	
76.67073	1000	15000	0.64746717	Cruz & Manning, 2015	
82.76011	1000	15000	0.61286464	Cruz & Manning, 2015	
17.81091	700	2000	0.59724173	Newton & Manning, 2000	
17.84761	800	10000	0.86304752	Newton & Manning, 2000	
20.44583	700	10000	0.88846959	Newton & Manning, 2000	
23.21144	700	4350	0.75380781	Newton & Manning, 2000	
27.66285	800	10000	0.85282439	Newton & Manning, 2000	
35.404	800	10000	0.84171497	Newton & Manning, 2000	
36.63419	700	15000	0.90215827	Newton & Manning, 2000	
37.21849	850	10000	0.82186175	Newton & Manning, 2000	
37.78992	700	2000	0.59743483	Newton & Manning, 2000	
38.32065	700	10000	0.84827353	Newton & Manning, 2000	
38.72262	600	10000	0.87220006	Newton & Manning, 2000	
38.74923	700	4350	0.71266584	Newton & Manning, 2000	
45.06785	800	10000	0.80101411	Newton & Manning, 2000	
49.66202	750	4350	0.7342934	Newton & Manning, 2000	
51.9617	700	4350	0.72606019	Newton & Manning, 2000	

52.02579	800	10000	0.77443287	Newton & Manning, 2000	
53.64258	900	10000	0.75366208	Newton & Manning, 2000	
56.67538	600	4350	0.7478661	Newton & Manning, 2000	
57.30202	700	15000	0.78544947	Newton & Manning, 2000	
57.33513	800	10000	0.7503106	Newton & Manning, 2000	
58.52461	800	10000	0.7446163	Newton & Manning, 2000	
58.8602	800	10000	0.74299482	Newton & Manning, 2000	
58.88503	850	10000	0.73708241	Newton & Manning, 2000	
58.90149	700	10000	0.75656024	Newton & Manning, 2000	
62.38953	700	4350	0.70484306	Newton & Manning, 2000	
63.47313	600	10000		Newton & Manning, 2000	L+H
64.03413	800	10000	0.71734559	Newton & Manning, 2000	
65.19489	700	15000		Newton & Manning, 2000	L+H
65.43301	600	4350	0.71561688	Newton & Manning, 2000	
69.80709	800	10000	0.6878685	Newton & Manning, 2000	
72.81551	800	10000	0.67236021	Newton & Manning, 2000	
74.11131	850	10000	0.66125499	Newton & Manning, 2000	
75.70124	800	10000	0.65734961	Newton & Manning, 2000	
76.64441	700	4350	0.64714581	Newton & Manning, 2000	
77.60163	700	2000	0.62547516	Newton & Manning, 2000	
78.03987	900	10000	0.63736974	Newton & Manning, 2000	
78.67212	800	10000	0.64149185	Newton & Manning, 2000	
79.62902	700	10000		Newton & Manning, 2000	L+H
82.65299	750	4350	0.61107723	Newton & Manning, 2000	
82.89606	800	10000		Newton & Manning, 2000	L+H
83.14389	850	10000	0.6118867	Newton & Manning, 2000	
85.85636	900	10000	0.59088307	Newton & Manning, 2000	
85.96352	850	10000	0.59269926	Newton & Manning, 2000	
90.98464	875	10000		Newton & Manning, 2000	L+H
6.9	800	9000	0.85947288	Shmulovich et al, 2001	
20.4	500	9000	0.88828567	Shmulovich et al, 2001	
20.4	650	9000	0.84222136	Shmulovich et al, 2001	
20.4	800	9000	0.84222136	Shmulovich et al, 2001	
24.9	800	5000	0.93389623	Shmulovich et al, 2001	
38.6	500	9000	0.73163606	Shmulovich et al, 2001	
42.7	800	9000	0.79655338	Shmulovich et al, 2001	
48	650	9000	0.81118423	Shmulovich et al, 2001	
48.1	800	5000	0.72254031	Shmulovich et al, 2001	
48.26	800	9000	0.78072143	Shmulovich et al, 2001	
60	800	9000	0.73288758	Shmulovich et al, 2001	
68.3	800	5000	0.66881081	Shmulovich et al, 2001	

70.3	800	9000	0.68239875	Shmulovich et al, 2001	
76	800	9000	0.653544	Shmulovich et al, 2001	
80	800	9000	0.63232125	Shmulovich et al, 2001	
1.445712	500	2000	0.70769414	Shmulovich et al, 2006	
1.451388	500	5000	0.87828522	Shmulovich et al, 2006	
2.839185	500	5000	0.88079814	Shmulovich et al, 2006	
5.270533	500	5000	0.88159352	Shmulovich et al, 2006	
5.511166	500	5000	0.88150389	Shmulovich et al, 2006	
5.532033	500	2000	0.72459054	Shmulovich et al, 2006	
6.879028	800	9000	0.85948811	Shmulovich et al, 2006	
7.272653	800	5000	0.72749298	Shmulovich et al, 2006	
7.807243	400	1000	0.73458117	Shmulovich et al, 2006	
8.252148	500	5000	0.87928313	Shmulovich et al, 2006	
9.999112	500	5000	0.87722172	Shmulovich et al, 2006	
14.99352	400	1000	0.75692638	Shmulovich et al, 2006	
16.33606	500	5000	0.86942065	Shmulovich et al, 2006	
20.07596	800	2000	0.53356338	Shmulovich et al, 2006	
20.39574	800	9000	0.84222634	Shmulovich et al, 2006	
20.39944	800	9000	0.84222202	Shmulovich et al, 2006	
22.51186	500	2000	0.75541515	Shmulovich et al, 2006	
22.77416	800	5000	0.73537316	Shmulovich et al, 2006	
28.82317	500	5000	0.86060044	Shmulovich et al, 2006	
30.89575	800	5000	0.71081929	Shmulovich et al, 2006	
31.36146	400	1000	0.77214484	Shmulovich et al, 2006	
33.55766	800	5000	0.69761918	Shmulovich et al, 2006	
35.26204	800	2000	0.51091009	Shmulovich et al, 2006	
37.79218	500	5000	0.84006392	Shmulovich et al, 2006	
43.12682	500	2000	0.74429219	Shmulovich et al, 2006	
43.61039	400	1000	0.77504338	Shmulovich et al, 2006	
48.09704	800	5000	0.72251628	Shmulovich et al, 2006	
48.26026	800	9000	0.78072061	Shmulovich et al, 2006	
50.87609	500	5000	0.80334542	Shmulovich et al, 2006	
56.54615	800	5000	0.69976445	Shmulovich et al, 2006	
57.87587	500	2000	0.74515593	Shmulovich et al, 2006	
58.17551	800	5000	0.69784899	Shmulovich et al, 2006	
68.30044	800	5000	0.66880918	Shmulovich et al, 2006	
70.30203	800	9000	0.68238856	Shmulovich et al, 2006	
76.00241	800	9000	0.65353161	Shmulovich et al, 2006	
80.00123	800	9000	0.63231447	Shmulovich et al, 2006	
0.581005	436	1800	0.7406766	Xie & Walther, 1993	
0.581005	402	1790	0.772384	Xie & Walther, 1993	

0.581005	467	1790	0.71242954	Xie & Walther, 1993	
0.581005	498	1765	0.68549011	Xie & Walther, 1993	
0.581005	530	1760	0.66244136	Xie & Walther, 1993	
0.581005	500	1750	0.68271138	Xie & Walther, 1993	
0.581005	563	1750	0.64144848	Xie & Walther, 1993	
0.581005	595	1725	0.55856889	Xie & Walther, 1993	

Supplemental Table 2: Calcite Data Base for Experimental Data of Mineral Solubility in H_2O-NaCl Fluids

Wt.% NaCl	T (°C)	P (bars)	ρ* (g/cm^3)	Source
12.65878	800	10000	0.87597266	Newton & Manning, 2002
27.12903	800	10000	0.85750521	Newton & Manning, 2002
33.23833	800	10000	0.85273086	Newton & Manning, 2002
36.21693	700	10000	0.86159041	Newton & Manning, 2002
38.91876	700	10000	0.85014001	Newton & Manning, 2002
40.83268	600	10000	0.86705469	Newton & Manning, 2002
44.41332	900	10000	0.78523826	Newton & Manning, 2002
45.02519	900	10000	0.78357613	Newton & Manning, 2002
45.159	900	10000	0.78322332	Newton & Manning, 2002
49.48695	800	10000	0.78886985	Newton & Manning, 2002
55.03733	700	10000	0.77953443	Newton & Manning, 2002
56.53902	800	10000	0.75784521	Newton & Manning, 2002
57.71643	600	10000	0.78773285	Newton & Manning, 2002
58.00525	700	14000	0.78165554	Newton & Manning, 2002
58.3766	900	10000	0.73752136	Newton & Manning, 2002
58.59103	700	6000	0.73876528	Newton & Manning, 2002
58.78769	900	10000	0.73566473	Newton & Manning, 2002
59.42635	600	10000	0.77989174	Newton & Manning, 2002
63.162	800	10000	0.72535178	Newton & Manning, 2002
67.01839	800	10000	0.70568681	Newton & Manning, 2002
67.40871	700	10000	0.71660091	Newton & Manning, 2002
71.20759	800	10000	0.68406674	Newton & Manning, 2002
72.46597	800	10000	0.67754207	Newton & Manning, 2002
74.66399	800	10000	0.6660897	Newton & Manning, 2002
75.9611	800	10000	0.65926933	Newton & Manning, 2002
79.48807	800	10000	0.64018933	Newton & Manning, 2002

Supplemental Table 3: Corundum Data Base for Experimental Data of Mineral Solubility in H_2O-NaCl Fluids

Wt.% NaCl	T (°C)	P (bars)	ρ* (g/cm^3)	Source	Notes
2.14	800	10000	0.8892	Newton & Manning, 2006	
6.49	800	10000	0.8874	Newton & Manning, 2006	
14.33	800	10000	0.8730	Newton & Manning, 2006	
26.43	800	10000	0.8581	Newton & Manning, 2006	
35.27	800	10000	0.8468	Newton & Manning, 2006	
48.79	800	10000	0.7916	Newton & Manning, 2006	
58.78	800	10000	0.7471	Newton & Manning, 2006	
68.36	800	10000	0.6988	Newton & Manning, 2006	
73.81	800	10000	0.6706	Newton & Manning, 2006	
79.20	800	10000	0.6418	Newton & Manning, 2006	
84.93	800	10000		Newton & Manning, 2006	L+H

Supplemental Table 4: Fluorapatite Data Base for Experimental Data of Mineral Solubility in H_2O-NaCl Fluids

Wt.% NaCl	T (°C)	P (bars)	ρ* (g/cm^3)	Source	Notes
10.69536	900	10000	0.8481	Antignano & Manning, 2008	
12.37618	800	15000	0.9430	Antignano & Manning, 2008	
16.98755	800	10000	0.8686	Antignano & Manning, 2008	
19.13252	800	15000	0.9284	Antignano & Manning, 2008	
29.55434	800	7000	0.7877	Antignano & Manning, 2008	
38.8375	800	10000	0.8270	Antignano & Manning, 2008	
40.37919	900	10000	0.8001	Antignano & Manning, 2008	
52.79127	900	15000	0.7867	Antignano & Manning, 2008	
57.15547	800	10000	0.7549	Antignano & Manning, 2008	
58.40078	800	15000	0.7678	Antignano & Manning, 2008	
58.5705	700	10000	0.7620	Antignano & Manning, 2008	
59.37938	800	7000	0.7271	Antignano & Manning, 2008	
59.90658	900	10000	0.7305	Antignano & Manning, 2008	
74.16192	900	15000	0.6702	Antignano & Manning, 2008	
75.45276	700	10000		Antignano & Manning, 2008	L+H
75.59205	800	7000	0.6531	Antignano & Manning, 2008	
77.18041	800	10000	0.6528	Antignano & Manning, 2008	
27.34662	800	10000	0.8573	Mair et al, 2017	
30.79615	800	10000	0.8548	Mair et al, 2017	
44.56819	800	10000	0.8067	Mair et al, 2017	
45.7976	800	10000	0.8026	Mair et al, 2017	
53.96734	800	10000	0.7697	Mair et al, 2017	
58.85801	800	10000	0.7467	Mair et al, 2017	
68.17172	800	10000	0.6998	Mair et al, 2017	
68.90335	800	10000	0.6960	Mair et al, 2017	
76.28846	800	10000	0.6575	Mair et al, 2017	
77.11129	800	10000	0.6532	Mair et al, 2017	

Supplemental Table 5: Fluorite Data Base for Experimental Data of Mineral Solubility in H_2O-NaCl Fluids

Wt.% NaCl	T (°C)	P (bars)	ρ* (g/cm^3)	Source
26.37992	800	10000	0.85809898	Tropper & Manning, 2007b
26.44256	800	10000	0.85804845	Tropper & Manning, 2007b
58.09246	800	10000	0.75043182	Tropper & Manning, 2007b
75.39382	800	10000	0.66226014	Tropper & Manning, 2007b